

3-16-2020

Use of UHPC Stay-In-Place Shells in Bridge Column Construction for Accelerated Bridge Construction

Nerma Caluk
ncalu001@fiu.edu

Follow this and additional works at: <https://digitalcommons.fiu.edu/etd>



Part of the [Structural Engineering Commons](#)

Recommended Citation

Caluk, Nerma, "Use of UHPC Stay-In-Place Shells in Bridge Column Construction for Accelerated Bridge Construction" (2020). *FIU Electronic Theses and Dissertations*. 4427.
<https://digitalcommons.fiu.edu/etd/4427>

This work is brought to you for free and open access by the University Graduate School at FIU Digital Commons. It has been accepted for inclusion in FIU Electronic Theses and Dissertations by an authorized administrator of FIU Digital Commons. For more information, please contact dcc@fiu.edu.

FLORIDA INTERNATIONAL UNIVERSITY

Miami, Florida

USE OF UHPC STAY-IN-PLACE SHELLS IN BRIDGE COLUMN CONSTRUCTION
FOR ACCELERATED BRIDGE CONSTRUCTION

A thesis submitted in partial fulfillment of the

requirements for the degree of

MASTER OF SCIENCE

in

CIVIL ENGINEERING

by

Nerma Caluk

2020

To: Dean John L. Volakis
College of Engineering and Computing

This thesis, written by Nerma Caluk, and entitled Use of UHPC Stay-In-Place Shells in Bridge Column Construction for Accelerated Bridge Construction, having been approved in respect to style and intellectual content, is referred to you for judgment.

We have read this thesis and recommend that it be approved

Ton-Lo Wang

Walled Orabi

Arindam Chowdhury

Atorod Azizinamini, Major Professor

Date of Defense: March 16, 2020

The thesis of Nerma Caluk is approved.

Dean John L. Volakis
College of Engineering and Computing

Andres G. Gil
Vice President for Research and Economic Development
and Dean of the University Graduate School

Florida International University, 2020

© Copyright 2020 by Nerma Caluk

All rights reserved.

ABSTRACT OF THE THESIS
USE OF UHPC STAY-IN-PLACE SHELLS IN BRIDGE COLUMN CONSTRUCTION
FOR ACCELERATED BRIDGE CONSTRUCTION

by

Nerma Caluk

Florida International University, 2020

Miami, Florida

Professor Atorod Azizinamini, Major Professor

This research utilizes Ultra-High Performance Concrete (UHPC) to construct prefabricated shells that act as stay-in-place forms for circular bridge columns. These innovative structural elements are intended to eliminate conventional formworks, reduce the on-site construction time, reduce life cycle costs, and improve the structural performance of bridge columns. The UHPC shell is placed around the column reinforcement assembled by using conventional methods, after which a UHPC step portion is cast at the column-to-footing interface to connect the UHPC shell with footing. Once the UHPC step portion has hardened, the conventional concrete is cast inside the shell. The final stage of construction involves placing and connecting a prefabricated cap-beam, using similar UHPC step connection. Two specimens were tested under constant axial load and incremental lateral load, until failure. The first specimen has reached the maximum value of 7.5% drift ratio, reaching a maximum lateral load capacity of 42 kips at 3% drift ratio when the UHPC shell cracked and the lateral capacity dropped 10%. No rebar rupture was recorded for the second specimen, but the test was completed at a drift ratio of 6% due to the significant drop in lateral load capacity.

TABLE OF CONTENTS

CHAPTER	PAGE
1 INTRODUCTION.....	1
1.1 Problem Statement	1
1.2 UHPC Properties	2
2 SYSTEM DEVELOPMENT.....	5
3 DESIGN AND CONSTRUCTION OF SPECIMENS.....	9
3.1 Design of the First Specimen	9
3.2 Construction of the First Specimen.....	11
3.3 Design of the Second Specimen.....	12
3.4 Construction of the Second Specimen	14
3.5 Pre-analyses for Both Specimens.....	15
4 TEST SETUP AND LOADING PROTOCOL	18
4.1 Test Setup and Protocol for Loading	18
4.2 Instrumentation.....	19
5 EXPERIMENTAL RESULTS	22
5.1 Results for the First Specimen	22
5.1.1 Damage Progression	22
5.1.2 Moment-Displacement Response	26
5.1.3 Drift-Rotation Response of the First Specimen	28
5.1.4 Energy Dissipation.....	29
5.1.5 Residual Drift.....	30
5.1.6 Strain Response.....	31
5.2 Results for the Second Specimen.....	33
5.2.1 Damage Progression	33
5.2.2 Moment-Displacement Response	38
5.2.3 Drift-Rotation Response	40
5.2.4 Energy Dissipation.....	41
5.2.5 Residual Drift.....	42
5.2.6 Strain Response.....	43

6	SUMMARY AND CONCLUSIONS	45
	REFERENCES	48

LIST OF TABLES

TABLE	PAGE
Table 1-1 Summary of applied loads and corresponding key damage states for first specimen [9].....	3
Table 3-1 Moment capacity of each section for first and second specimen and their ratios.....	16
Table 4-1. Instrumentation summary	20
Table 5-1 Summary of applied loads and corresponding key damage states for first specimen	25
Table 5-2 Summary of applied loads and corresponding key damage states for second specimen	37

LIST OF FIGURES

FIGURE	PAGE
Figure 1-1 Work on circular columns using formwork and scaffolding.	2
Figure 2-1 Location of the reinforcement: a) first specimen, b) right specimen.	7
Figure 2-2 Connecting prefabricated bridge columns using UHPC and spliced reinforcement: a) seismic connection, b) non-seismic connection [20].	8
Figure 3-1 Details of the first specimen.	10
Figure 3-2 Construction sequence of the first specimen: a) footing reinforcement; b) prefabricated UHPC shell; c) UHPC step connection; d) casting of the NSC; e) connecting the specimen to the loading actuator; f) final test setup.	12
Figure 3-3 Details of the second specimen.	14
Figure 3-4 Construction sequence of the second specimen: a) footing reinforcement including dowel bars; b) steel cage; c) prefabricated UHPC shell with the embedded longitudinal reinforcement; d) UHPC shell connection with the footing using UHPC step; e) complete specimen; f) test setup of the second specimen.	16
Figure 3-5 Moment-curvature curves for both UHPC shell column section and equivalent conventional column	17
Figure 4-1 Test setup for first and second specimen.	18
Figure 4-2 Loading protocol for lateral load.	19
Figure 4-3 Instrumentation plan for the first specimen. a) string potentiometers and displacement transducers for displacement and rotational measurements; b) strain gauges location on column reinforcement and dowel bars.	21
Figure 4-4 Instrumentation plan for the second specimen. a) string potentiometers and displacement transducers for displacement and rotational measurements; b) strain gauges location on column reinforcement and dowel bars.	21
Figure 5-1 Damage progression of the first specimen: a) 0.5% drift ratio; b) 1% drift ratio; c) 1.5% drift ratio; d) 2% drift ratio; e) 3% drift ratio; f) 6% drift ratio; g) 7.5% drift ratio; h) final damage of the specimen after the instrumentation removal.	25
Figure 5-2 Moment-displacement response of the first specimen and the conventional column specimen.	27
Figure 5-3 Comparison of response envelopes of the first specimen and the conventional column specimen.	27
Figure 5-4 Drift-rotation response of the first specimen.	29
Figure 5-5 Energy dissipation at each drift level of the first specimen.	30
Figure 5-6 Residual drift after each drift ratio application for the first specimen.	31

Figure 5-7 Strain distribution on the north longitudinal and dowel bars for first specimen.	32
Figure 5-8 Damage progression of the second specimen: a) 0.5% drift ratio; b) 1% drift ratio; c) 1.5% drift ratio; d) 2% drift ratio; e) 3% drift ratio; f) 4% drift ratio; g) 5% drift ratio; h) 6% drift ratio.	38
Figure 5-9 Moment-displacement response of the second specimen and the first specimen for comparison.	39
Figure 5-10 Comparison of response envelopes for both specimens.	40
Figure 5-11 Drift-rotation response for the second specimen.	41
Figure 5-12 Energy dissipation comparison of both specimens.	42
Figure 5-13 Residual drift ratio for the second specimen and the comparison to the first specimen.	43
Figure 5-14 Strain distribution on the south longitudinal and dowel bar for the second specimen.	44

1 INTRODUCTION

1.1 Problem Statement

The most common method for supporting the self-weight of wet concrete and its fluid pressure, machines, and workers is the use of conventional formwork and scaffolding. In order to gain access to the structure under construction, conventional scaffolding is typically used. Figure 1-1 shows scaffolding and formwork in bridge site. However, placing and erecting the formwork and scaffolding components usually take time, leading to an increase in construction cost and traffic congestions. Furthermore, possible failure of formwork and scaffolding should be considered due to the unexpected site conditions and deviations from the original design [1]. A common cause of the failure of formwork and scaffolding is the underutilization of hardware, due to rushing of the erection process [2]. If the failure of formwork occurs during a concrete pour, concrete might start to leak, leading to possible structural collapse, injuries or fatalities. Several interviews had been conducted in order to determine the most common formwork and falsework failures which include lack of planning, stripping of formwork, falling objects, floor collapse and material mishandling [3]. Another cause of formwork failure is due to possible human errors or crushing of wooden surface where the heavy loads are located if appropriate bearing surface of joints is not provided. According to the “*Use and Re-use of Formwork: Safety Risk and Reliability Assessment*” report, the formwork being re-used is not factored into its design which leads to possible degradation of its structural capacity when exposed to different loads [4].



Figure 1-1 Work on circular columns using formwork and scaffolding.

To avoid and prevent possible formwork and scaffolding failures, a new concept has been developed at Florida International University, implementing ultra-high performance concrete (UHPC), by the PI, to prefabricate shells that act as stay-in-place forms for bridge elements such as bridge columns [5, 6]. The prefabricated shell is intended to eliminate excessive formwork while acting as a durable protective layer against the environmental attacks for the conventional concrete located inside while also reducing the on-site construction time and traffic congestion. Similar research has been conducted where similar UHPC shell concept was implemented in cap beams, in which Azizinamini et al., [7] shows detailed experimental results together with a comparison of a cap beam made of UHPC shell element and identical cast-in-place cap beam.

1.2 UHPC Properties

Ultra-high performance concrete (UHPC) is known for its flowability which means that its properties and features allow for shaping of innovative structural elements such as thin shells and filling connections with tight tolerances, therefore making UHPC a perfect material for accelerated bridge construction (ABC) applications. UHPC consists of a

combination of Portland cement, silica fume, fine sand, high-range water-reducing admixture (HRWR), water, and steel fibers (Table 1-1). The diameter of the cylindrical, nondeformable steel fibers that are part of UHPC is 0.008 inches with a length of 0.5 inches. The proportion of steel fibers ranges from 2% to 4% by volume. This cementitious-based composite material can reach a compressive strength above 22 ksi and tensile strength above 725 psi which is more than 5 times the compressive strength and about 2 times more than the tensile strength of normal concrete [8]. Furthermore, it has been proved that UHPC has an excellent bond strength to roughened concrete substrates [9]. In comparison to conventional concrete, UHPC also poses greater frost and salt decay salt resistance, a lower rate of carbonation, and higher chloride resistance. Thus, structural elements made from UHPC will have lower maintenance and service life cost [10].

Table 1-1 Summary of applied loads and corresponding key damage states for first specimen [9].

Material	Amount (lb/yd ³)	Percent by Weight
Portland Cement	1,328	31.5
Silica Sand	1,288	30.5
Ground Quartz	367	8.7
Silica Fume	518	12.3
Superplasticizer	23	0.5
Steel Fibers	416	9.9
Water	278	6.6

Previous research projects have been conducted at Florida International University on UHPC shell elements, where a thin layer of UHPC shell was effectively used for repairing and retrofitting of damaged bridge elements, resulting in an 18% increase in capacity of

the retrofitted element [11, 12]. Implementation of UHPC shell elements in new bridge construction can be compared to the use of fiber-reinforced polymer (FRP) tubes and concrete-filled steel tubes (CFSTs). Both the FRP tubes and CFSTs are used to increase the strength and stiffness of the bridge element while also speeding up the process of construction. These elements are known to provide efficient and economical alternatives in bridge column construction; however, their field implementation is limited due to unreliable connection, especially in seismic zones. Furthermore, CFSTs are also susceptible to rapid corrosion of steel tubes caused by aggressive environments [13, 14]. The advantage of FRP tubes includes their resistance to corrosion, being lightweight and having high strength but the presence of concrete shrinkage, poor fire resistance and inadequate concrete compaction due to the weak interface between the conventional concrete and FRP tubes reduce its load-bearing capacity [15, 16]. Furthermore, brittle failure of FRP tubes is present by fracturing FRP laminates which is not a desirable mode of failure for bridge columns. The use of precast UHPC shell prevents the corrosion of the reinforcement, protects the normal concrete core from the environmental attacks, while also showing a predictable ductile failure.

2 SYSTEM DEVELOPMENT

Rapid deterioration is one of the most common factors that cause bridges to be structurally deficient or functionally obsolete. Almost 10% of bridges in the United States are considered to be structurally deficient and around 13.6% are functionally obsolete. Furthermore, it has been also estimated that about 15% of U.S. bridges were built between 40 and 49 years ago which means that they will soon reach their end of functional lifespan [17]. The use of more durable material, in this case UHPC, and implementing it in precast elements can extend the service life of bridge elements in comparison to the service life of bridge elements made out of conventional concrete. Many chloride penetration tests were conducted by Graybeal [18] which included ponding of a 3% sodium chloride solution on the surface of the concrete. After the 90-day period during which the UHPC surface was exposed to the solution, penetration of the chloride into the concrete was determined. As the results predicted, the higher concentration of the chloride ions was observed at the surface. However, only a small amount of the chloride solution was recorded to penetrate through the UHPC. Based on Graybeal's research and the results [18], it has been proved that the mechanical properties of UHPC should act as a protective layer for the bridge elements from severe environments and corrosion for steel reinforcement usually caused by carbonation. Other research on chloride penetration was done at Florida International University, concentrating on the effect of corrosion macro-cells that can be developed between normal strength concrete (NSC) substrate and the repair area of the UHPC. Based on Farzad et al., [19], repairing concrete bridge columns with UHPC generally improved the bond strength between substrate and repair materials. Furthermore, together with the low permeability of UHPC, this kind of repair can result in more durable structural

elements, improving the service life of the element. This is accomplished by obstructing the ingress of damaging agents.

Once axial and lateral loads have been applied to a conventional reinforced concrete column, together with the moisture ingress through concrete, corrosion of the reinforcement starts, causing the expansion of steel bars and crack formation, resulting in the concrete to spall off. The area of the existing column section then starts to decrease, together with its lateral load capacity. To prevent the spalling of column concrete and reduction of the design strength, a prefabricated UHPC shell was incorporated and two specimens were tested at Florida International University. No reinforcement was embedded inside the UHPC shell for the first specimen, whereas a steel cage was only placed in the normal concrete core. Since the UHPC is cast first, the UHPC surface is smooth, therefore, the friction between the conventional concrete and the shell might be reduced, causing material slippage due to the excessive lateral loads. Due to this possible issue, the second specimen was envisioned. The second specimen consisted of longitudinal reinforcing bars partially embedded in the UHPC shell, while being shared with the column concrete and the transverse reinforcement (spirals) was fully embedded in the UHPC shell. This detail was envisioned to prevent possible slippage, causing better interaction and bonding between two materials. Figure 2-1. Show schematics for the first and second specimens.

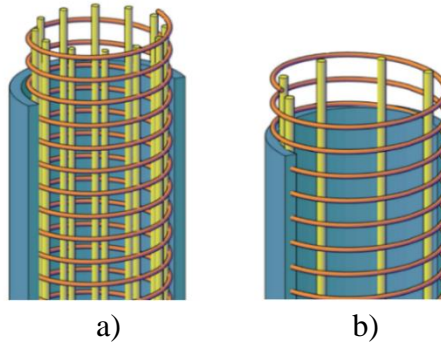


Figure 2-1 Location of the reinforcement: a) first specimen, b) right specimen.

The UHPC shell is connected to adjoining elements (footing or cap beam) by splicing the longitudinal reinforcing bars with dowels extended from the adjoining elements. In order to shorten the splice length of the bars and shift the formation of the plastic hinge away from the adjoining elements and their interfaces with the shell, UHPC is also implemented in the connection between the column section and the adjoining elements (footing or cap beam). Previous research was conducted at Florida International University on prefabricated columns emulating reinforced concrete columns with seismic and non-seismic details where UHPC was utilized in the connection between prefabricated substructure elements (columns to footing or cap beam). For the seismic detail, two layers of UHPC were incorporated, while for the non-seismic detail, only one layer was incorporated, as shown in Figure 2-2 [20]. Once tested, the specimen experienced the formation of the plastic hinge between the two layers of UHPC for the seismic detail, while for the non-seismic design, plastic hinge has shifted away from UHPC connection detail, proving that this advanced material can be successfully used to shift the plastic hinge location as needed. Furthermore, the use of UHPC in the locations of a splicing region was proven to be more effective, where the development and lap splice lengths of the reinforcing bars were shorter if compared to those developed in normal strength concrete.

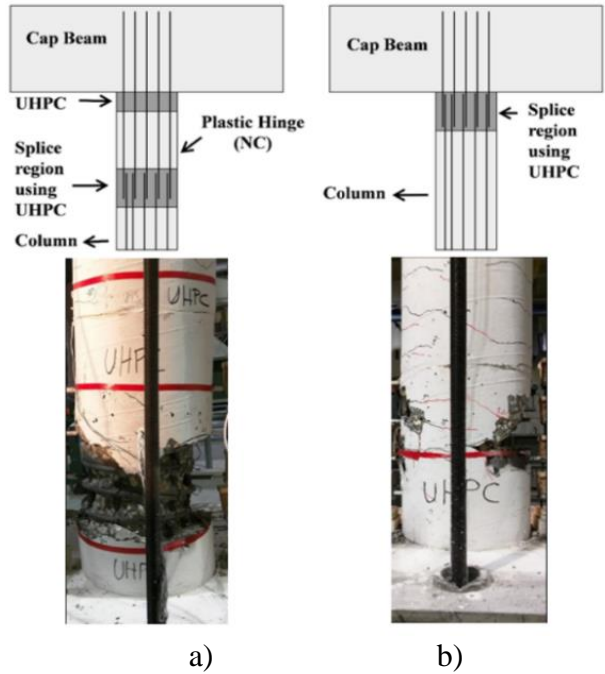


Figure 2-2 Connecting prefabricated bridge columns using UHPC and spliced reinforcement: a) seismic connection, b) non-seismic connection [20].

3 DESIGN AND CONSTRUCTION OF SPECIMENS

In this research project, two column specimens consisting of a prefabricated UHPC shell were designed, constructed and tested at Florida International University. Both specimens consisted of longitudinal and transverse reinforcement where the UHPC contained 2% steel fiber by volume. The cavity of the UHPC shells was filled with normal strength concrete. A step made of UHPC was used to connect the column to the footing, in which the splicing region was located. The main goal of the UHPC step detail is to shift the plastic hinge away from the footing-to-column interface, keeping the footing uncracked and meeting its requirement of being a capacity protected element. A similar UHPC connection can be utilized between the cap beam and the column.

3.1 Design of the First Specimen

The first specimen was designed to have no reinforcement embedded in the UHPC shell, with the conventional steel cage located inside the inner part of the column, in the normal strength concrete. The specimen footing consisted of a conventional steel cage with #5 longitudinal reinforcing bars and normal strength concrete. The specimen had a 16 in. outer diameter UHPC shell, with 1 in. wall thickness and 12#5 longitudinal bars spliced with a set of 12#5 dowel bars, extending from the footing. #3 spiral was used in the steel cage as the transverse reinforcement, with a diameter of 13 in. and 2.5 in. pitch spacing. The same spiral was used for the transverse reinforcement of the dowel bars located in the footing. No transverse reinforcement was used within the UHPC step section due to the higher shear capacity of that section, and ductility provided by the steel fibers from the UHPC shell. The diameter of the UHPC step was 21 in. with height of 7 in.

Based on the UHPC design specifications [23], in which the lap splice length is defined as eight times the bar diameter, it was found that 5 in. was the sufficient length to splice column longitudinal reinforcement with the dowel bars extended from the footing. Besides the lap splices, another set of 12#5 dowel bars were located and developed in the outer perimeter of the UHPC step, but not in the UHPC shell. These dowel bars were intended to prevent any possible detachment of the UHPC step from the footing, which might cause racking of the column when the cyclic load is applied. The effective height of the first specimen (from the center of the applied load to the footing interface) was 69 in. Figure 3-1 shows the full reinforcement details of the first specimen. Section A-A and B-B in Figure 3-1 show the cross-sections of the reinforcement details of the UHPC step section and the column section, respectively.

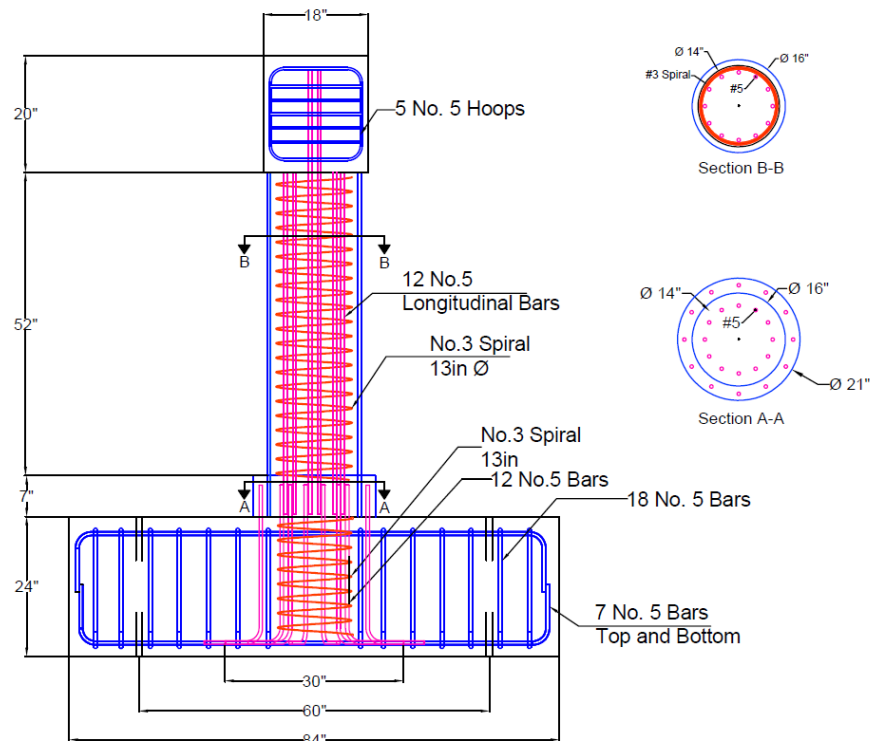


Figure 3-1 Details of the first specimen.

3.2 Construction of the First Specimen

The construction of the first specimen started by the assembly and placement of the footing reinforcement together inside the formwork along with the two sets of extended dowel bars, as shown in Figure 3-2a. Normal strength concrete was cast in the footing formwork then UHPC shell construction started. A sonotube of a diameter same as the outer diameter of the shell (16 in.) was used to shape the outer perimeter of the prefabricated shell, while Styrofoam was used to form the inner perimeter and the 1-in. uniform shell wall thickness. Once the UHPC of the shell hardened, both Styrofoam and the sonotube were removed to form the shell shown in Figure 3-2b. As mentioned in the previous section, no reinforcement was embedded in the prefabricated shell element, whereas the column transverse and longitudinal reinforcement (steel cage) were placed in the UHPC shell cavity. During the construction process, the steel cage had to be placed inside the UHPC shell and placed together on top of the footing due to the laboratory height limitations. It should be noted that in the field construction, UHPC shell and steel cage can be lifted and placed separately on the footing element. Once both the UHPC shell and steel cage have been placed on the top of the footing, longitudinal reinforcement was spliced with the first set of the dowel bars extending from the footing. In order to shape the UHPC step, another sonotube with a height of 7 in. was used which was cast after the reinforcement splicing was completed, as shown in Figure 3-2c). Once the UHPC step hardened, normal strength concrete was cast in the shell cavity with the loading cap, as shown in Figure 3-2d. After the curing of normal strength concrete, the specimen was moved to the final test setup position, as shown in Figure 3-2e and Figure 3-2f.

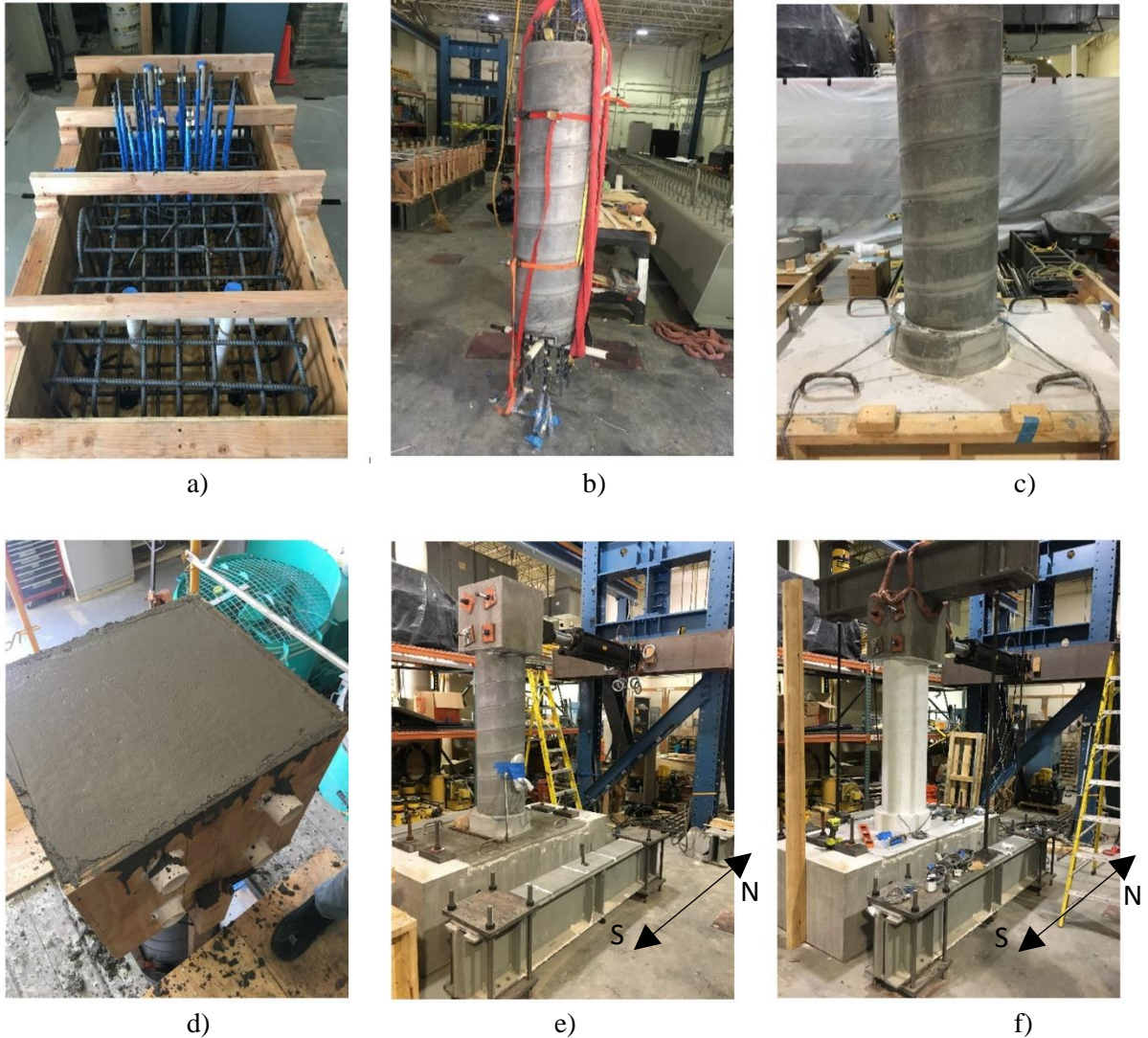


Figure 3-2 Construction sequence of the first specimen: a) footing reinforcement; b) prefabricated UHPC shell; c) UHPC step connection; d) casting of the NSC; e) connecting the specimen to the loading actuator; f) final test setup.

3.3 Design of the Second Specimen

The second specimen was designed with two main differences in comparison to the first specimen. The first difference is that the column longitudinal reinforcement is partially embedded in the UHPC shell, while also being exposed to the normal concrete core in order to develop a better bond between the two materials. This detail was added due to the smooth surface of UHPC once hardened and potentially reduced friction between NSC and UHPC,

where it was assumed that possible slippage may occur between the two materials once the cyclic loading is applied. The second difference is the location of the spiral, which was completely embedded in the UHPC shell, around the partially embedded longitudinal bars. Since bigger reinforcing bar diameter was needed for the bar to be shared between NSC and UHPC, 8#6 bars were used for the longitudinal reinforcement instead of 12#5 bars, as used for the first specimen, where a similar area of steel was used. For transverse reinforcement, #3 spiral of 14.5 in. diameter was used, with 2.5 in. pitch spacing. For the dowel bars, #3 spiral was used, however, the diameter was smaller, corresponding to 13 in. Same diameter of the shell (16 in.) and shell wall thickness (1 in.) were incorporated to match the first specimen in order to appropriately compare the results of both specimens. Similar to the first specimen, a UHPC step was used to connect the UHPC shell to the footing where the splicing region was located. No transverse reinforcement (spirals) was used within the UHPC step. Since #6 longitudinal bars were used, the splicing region increased from 5 in. to 6 in. [21] while the UHPC step height increased to 7.5 in. but the outer diameter of the UHPC step remained the same as 21 in. The longitudinal reinforcement of the column was spliced with 8#6 dowel bars extended from the footing. Another set of 8#5 dowel bars was used at the outer perimeter of the UHPC step in order to prevent possible separation between the UHPC step and the footing. Same dimensions of the footing with the same steel cage footing arrangement were incorporated for the second specimen. The column effective height remained the same as the first column, 69 in. Figure 3-3 shows the reinforcement details of the second specimen. Section A-A and B-B, in Figure 3-3, shows the reinforcement details for UHPC step section and column section with UHPC shell.

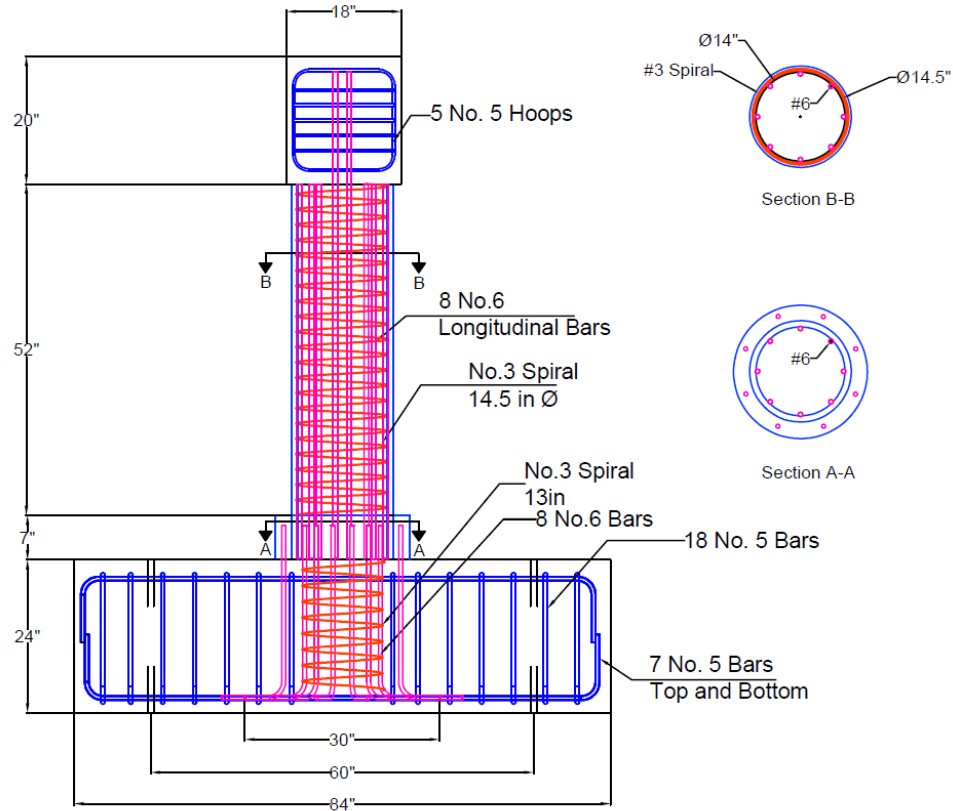


Figure 3-3 Details of the second specimen.

3.4 Construction of the Second Specimen

The construction of the second specimen started in a similar way as the first specimen. For footing construction, footing reinforcement was placed inside the formwork with only one difference from the first specimen, in the arrangement of the two sets of extended dowel bars as shown in Figure 3-4a (12#5 for the first specimen vs 8#6 for the second specimen) then the footing was cast with the normal strength concrete. The construction of the UHPC shell for the second specimen started by acquiring Styrofoam piece with eight partially opened holes at its perimeter, where the 8#6 longitudinal bars were placed around which the transverse reinforcement spiral was set, creating one element, as shown in Figure 3-4b. The element was then inserted into a 16-in diameter sonotube which shaped the outer

perimeter of the shell. After its placement, the UHPC was cast. Once the UHPC hardened, the Styrofoam and sonotube were removed, as shown in Figure 3-4c, and the UHPC shell element was placed on the top of the footing and the longitudinal reinforcing bars were then spliced with the dowel bars extended from the footing. Using another sonotube of 7.5 in. in height and 21 in. in diameter, UHPC step was shaped and cast, as shown in Figure 3-4d, similarly to the first specimen. After the UHPC step hardened, the final phase of the construction was conducted which involved casting of normal strength concrete inside the UHPC shell cavity and the loading cap, as shown in Figure 3-4e. The final test setup of the second specimen is shown in Figure 3-4f.

3.5 Pre-analyses for Both Specimens

Prior to testing the specimens, moment-curvature analyses were conducted on the column section (Section B-B in Figures 3-1. and 3-3.), UHPC step section (Section A-A in Figures 3-1. and 3-3.) and footing section of both specimens. In order to predict the failure region and confirm the shift of the plastic hinge away from the footing-to-column interface, a preliminary analysis had to be done. Figure 3-5 represents the moment-curvature plots for column section of both specimens and an equivalent conventional column of the same diameter for comparison purpose. Based on the results from the plot, it can be concluded that the section comprised of UHPC shell shows higher moment capacity in comparison to the conventional section, resulting in an increase of about 10%. Table 3-1 shows the moment capacities of three section for both specimens together with the moment ratios (UHPC step or footing moment capacity divided by the column moment capacity), predicting that the damage is to be expected in the column section for both cases.

Table 3-1 Moment capacity of each section for first and second specimen and their ratios

Specimen	Column Section	UHPC Step Section		Footing Section	
	Moment, M_1 (kip-ft)	Moment, M_2 (kip-ft)	Ratio M_2/M_1	Moment, M_3 (kip-ft)	Ratio M_3/M_1
First specimen	1403.45	4443.47	3.17	3014.68	2.15
Second specimen	1446.73	3893.94	2.69	3014.68	2.08



a)



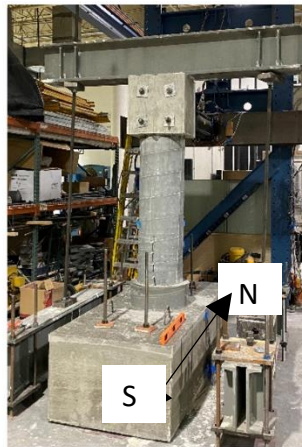
b)



c)



d)



e)



f)

Figure 3-4 Construction sequence of the second specimen: a) footing reinforcement including dowel bars; b) steel cage; c) prefabricated UHPC shell with the embedded longitudinal reinforcement; d) UHPC shell connection with the footing using UHPC step; e) complete specimen; f) test setup of the second specimen.

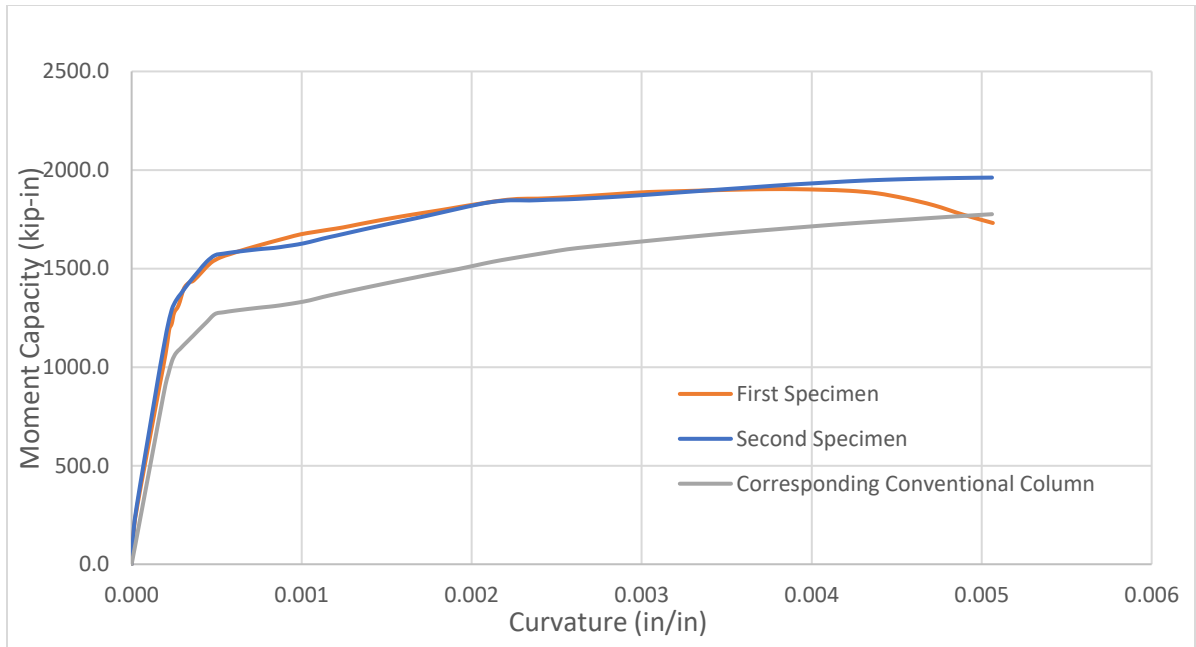


Figure 3-5 Moment-curvature curves for both UHPC shell column section and equivalent conventional column

4 TEST SETUP AND LOADING PROTOCOL

4.1 Test Setup and Protocol for Loading

In this research project, both specimens were tested under incremental lateral cyclic loading using a 110-kip hydraulic ram and constant axial load of 120 kips using two hydraulic jacks located on a spreader beam placed horizontally on top of the specimen. The hydraulic ram that was used for lateral displacement was attached to a steel beam, bolted to the two-column frame on the north side, as shown in Figure 4-1.

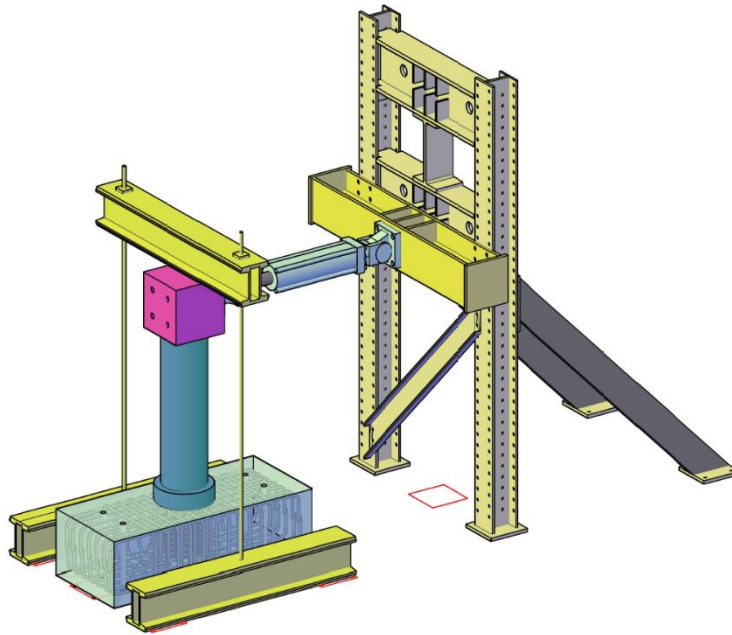


Figure 4-1 Test setup for first and second specimen.

For both tests, a cantilever model type was used where the inflection point was assumed to be at the mid-height of the actual column with a fixed-fixed condition. For this case, the plastic deformations should be concentrated around the plastic hinge zone which was located above the UHPC step. Using the described test setup, the following data were

obtained for experimental results analysis and comparison: lateral forces, moments, curvatures, rotations, strains, and displacement for both specimens.

The idealized yield displacement was based on a bilinear model and was determined by initially applying low displacement cycles. An equivalent elastoplastic system was assumed for the yielding displacement (Δ_y). After the yield displacement was obtained, the column was subjected to three cycles of $2\Delta_y$, $3\Delta_y$, $4\Delta_y$ and so on, as shown in Figure 4-2. After each cycle, cracks were traced, and the observed damage was documented. The testing of both specimens was completed once rebar rupture occurred or significant loss in lateral capacity.

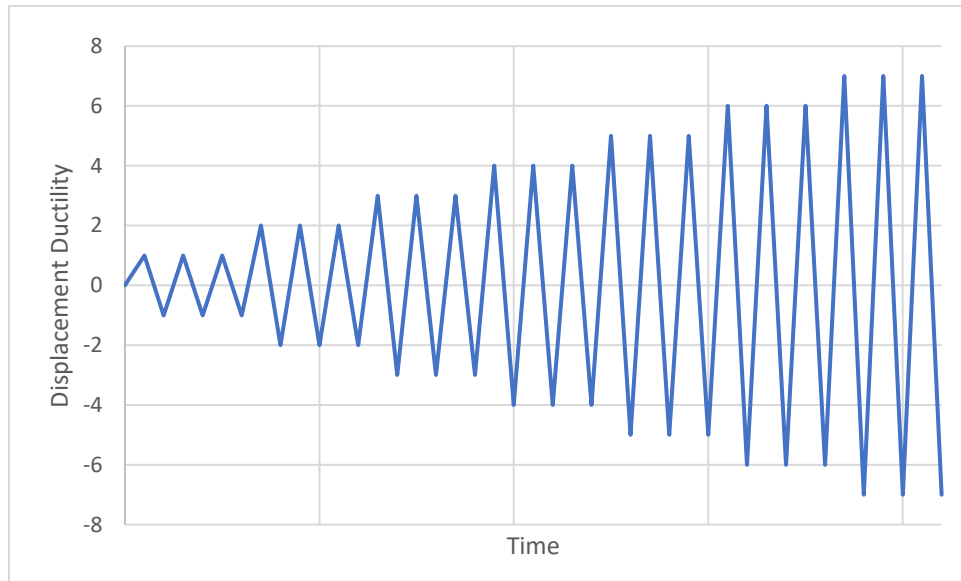


Figure 4-2 Loading protocol for lateral load.

4.2 Instrumentation

The specimens were extensively instrumented using strain gauges for reinforcement, load cells, string potentiometers, displacement transducers, and recoding cameras in order to closely monitor and evaluate the behavior of each specimen. Table 4-1 lists all the

instruments used for each specimen. Several different observations, notes and measurements were made during the testing of each specimen which includes cracking patterns, loading vs. displacement graph, curvatures, drift ratios and maximum strain values. For the first specimen, 24 different strain gauges were placed at different locations: 12 strain gauges on the longitudinal reinforcement of the column, and 12 strain gauges inside the footing. The strain gauges, located below the footing interface, were applied to the dowel bars, right below the surface, in the loading direction where tension and compression in these bars are expected. Four displacement transducers were attached to the UHPC step at two perpendicular directions (North, South, East, and West) to monitor the rotation between the UHPC step and the footing. Another four pairs of displacement transducers were instrumented on the south and north side of the column, in the direction of the loading, to record the rotation of the specimens when subjected to cyclic lateral loading. Furthermore, four string potentiometers were located on the south side of the column, at heights of 26.5 in, 38.5 in., 40.5 in., and 68.25 in., measured from the top of the footing, in order to measure the displacement of the column during the load application. Four recording cameras were placed on all four sides of each specimen, simultaneously recording the displacement and damage progression of each specimen. Figure 4-3 and Figure 4-4 show the instrumentation plan for the first and second column, respectively.

Table 4-1 Instrumentation summary.

Instrumentation	First Specimen	Second Specimen
	Count	Count
Displacement String Potentiometers	4	4
Displacement transducers for rotation and curvature	12	8
Longitudinal Reinforcement Strain Gauges	12	8
Dowel Reinforcement Strain Gauges	12	6
Actuator load cell	1	1
Cameras	4	4

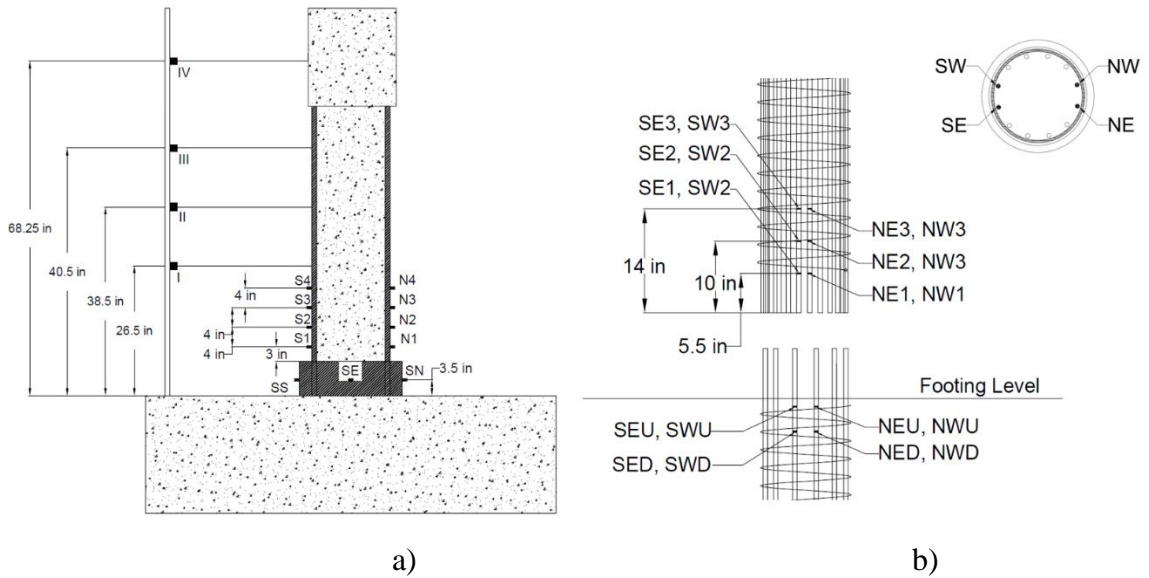


Figure 4-3 Instrumentation plan for the first specimen. a) string potentiometers and displacement transducers for displacement and rotational measurements; b) strain gauges location on column reinforcement and dowel bars.

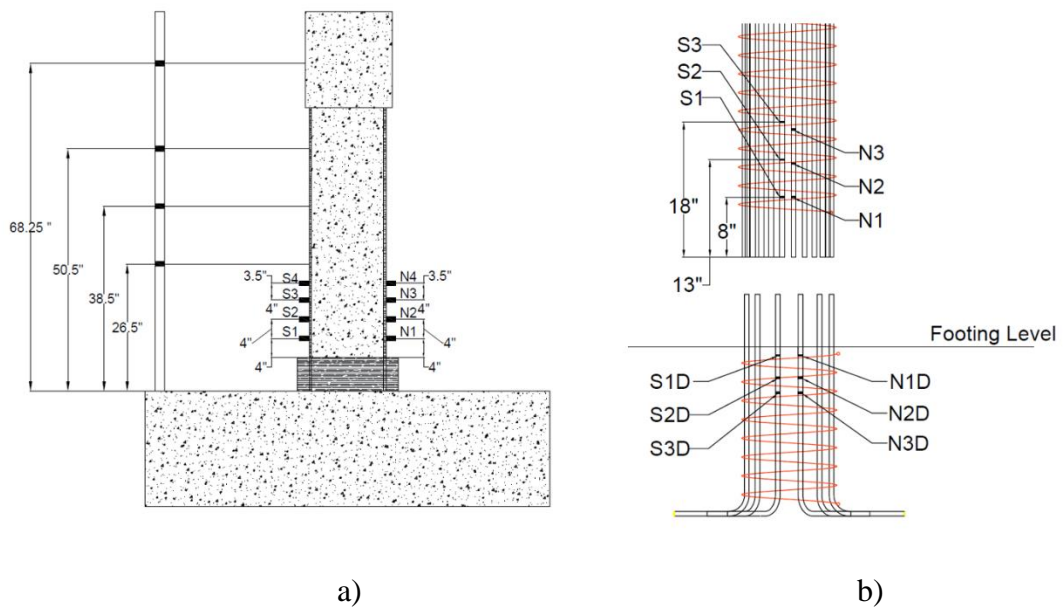


Figure 4-4 Instrumentation plan for the second specimen. a) string potentiometers and displacement transducers for displacement and rotational measurements; b) strain gauges location on column reinforcement and dowel bars.

5 EXPERIMENTAL RESULTS

5.1 Results for the First Specimen

5.1.1 Damage Progression

Based on the low displacement cycles, the yield displacement (Δ_y) was found to be 0.35 in., which corresponds to 0.5% drift ratio, and an applied lateral load of 27 kips (pushing from North to South). When the load was applied in the opposite direction (pulling from South to North) to cause the same yield displacement, the magnitude was found to be 32 kips. For the second and third cycles of Δ_y , a load of 30 kips was reached on both loading directions. Only minor cracks were observed and located on the interface between the UHPC shell and the UHPC step and around the holes made for the displacement transducers, as shown in Figure 5-1a.

The next displacement corresponded to $2\Delta_y$ (0.7 in.) and was applied in both loading directions, causing a drift of 1%. A lateral load of 38 kips was recorded on the positive side (pushing from North to South), however, for the negative side (pulling from South to North), a lateral load of 40 kips was recorded. For the second and third cycles corresponding to the same displacement, loads of 35 kips and 38 kips were reached on the positive and negative sides, respectively. The progression of the cracks was observed around the column during the load application, while being mostly concentrated on the interface between the UHPC step and UHPC shell as shown in Figure 5-1b.

The $3\Delta_y$ displacement was then applied in both loading directions with a load of 40 kips for the first cycle, 37 kips for the second cycle, and 36.5 kips for the third cycle. This displacement had a value of 1.05 in. and corresponds to a drift ratio of 1.5% where further

opening of exiting cracks had continued. At this point, the steel fibers were visible at the interface between the UHPC shell and UHPC step where the largest cracks were observed, mostly concentrated on the south side of the column, as shown in Figure 5-1c.

At a drift ratio of 2% (displacement of 1.4 in.), a lateral load of 39 kips was reached for the first two cycles. At the third cycle, the load dropped down to 36 kips when the load was applied from North to South with structural cracks and minor spalling of UHPC shell, as shown in Figure 5-1d.

The next drift ratio applied had a value of 3% (displacement of 2.1 in) with a lateral load of 42 kips for the first cycle. Once the load was fully applied, a loud noise was heard, indicating the cracking of the shell and its separation from the UHPC step. Right after this loud sound, the load dropped down to 37.5 kips when the load was applied from North to South. The same displacement was applied in the opposite direction (pulling from North to South), however, no cracking of UHPC shell was observed. For the second and third cycles, a lateral load of 30 kips was applied to accomplish the same displacement for the positive side (pushing from North to South) while the negative side needed larger load magnitude, corresponding to 40 kips. The spalling of the UHPC was observed, being mostly concentrated at the interface of the UHPC shell and UHPC step, as shown in (Figure 5-1e).

Since no bar rupture occurred, the testing was resumed with the application of 4% drift ratio (displacement of 2.8 in.). For the first cycle, lateral loads of 31 kips and 40 kips were applied for positive side (pushing from North to South) and negative side (pulling from South to North), respectively whereas for the second and third cycles the lateral load

dropped to 28 kips for the positive side and 35 kips for the negative side. No significant additional damage was observed.

For the following drift ratio of 6% (displacement of 4.2 in.), four cycles were applied where the lateral load for the first cycle reached 30 kips and 34 kips and then dropped down to 26 kips and 30 kips, for positive and negative sides, respectively. The progression of cracking continued but no rupture was observed (Figure 5-1f).

A drift ratio of 7.5% was reached next, corresponding to a displacement of 5.2 in. and lateral loads of 28 kips and 32 kips for positive and negative sides, respectively. When the pulling load was applied to the specimen, a loud sound was heard marking the rupture of one of the reinforcing bars on the south side of the column, after which the test was marked complete. Figure 5-1g presents the damage of the tested specimen (when pulled from South to North) where an opening of about 1.6 in. can be observed on the south side of the specimen. Figure 5-1h shows the final damage after the removal of instruments. The summary of the loadings and key damage states is listed in Table 5-1.

Table 5-1 Summary of applied loads and corresponding key damage states for first specimen.

Displacement Ductility	Number of Cycles	Drift Ratio	Maximum Lateral Load	Key Damage Stage
Δ_y	3	0.5%	32 kips	Minor cracks at Interface between column and UHPC shell
$2\Delta_y$	3	1%	38 kips	Progression of minor cracks at Interface between column and UHPC shell
$3\Delta_y$	3	1.5%	40 kips	Further opening of exiting cracks Steel fibers were noticed
$4\Delta_y$	3	2%	39 kips	Large cracks and minor spalling
$6\Delta_y$	3	3%	42 kips	Shell cracked at north side Damage concentrated at Interface between column and UHPC shell
$8\Delta_y$	3	4%	31 kips (N to S) 40 kips (S to N)	Same damage as 3% Drift Ratio
$12\Delta_y$	4	6%	30 kips (N to S) 34 kips (S to N)	Large opening between column and UHPC shell
$15\Delta_y$	2	7.5%	28 kips (N to S) 32 kips (S to N)	Bar rupture at south side

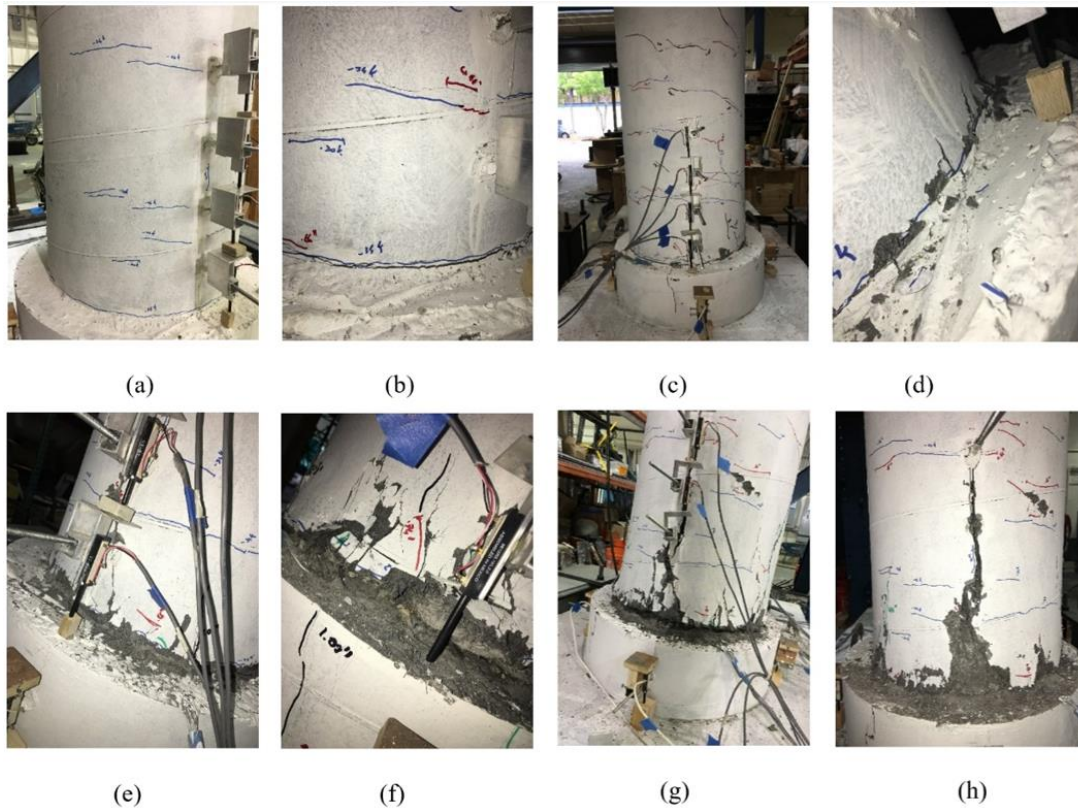


Figure 5-1 Damage progression of the first specimen: a) 0.5% drift ratio; b) 1% drift ratio; c) 1.5% drift ratio; d) 2% drift ratio; e) 3% drift ratio; f) 6% drift ratio; g) 7.5% drift ratio; h) final damage of the specimen after the instrumentation removal.

5.1.2 Moment-Displacement Response

Based on the measurements collected from the first specimen, a moment-displacement hysteresis loops for the cyclic response are plotted in Figure 5-2. The same figure also shows similar results for a conventional column that has the same dimensions with no UHPC implementation [22]. In addition, response envelopes for the first specimen and the conventional column are shown in Figure 5-3. Based on these graphs, it can be noted that the load suddenly dropped at 3% drift ratio (displacement of 2.1 in) on the positive side when a loud cracking sound was heard. This sudden drop indicated the separation of the UHPC shell from the UHPC step when the column was pushed from North to South which is shown in the later cycles for higher drift ratios. From this graph, it can be also observed that the negative side maintained the full capacity throughout the test even after reaching a drift ratio of 7.5%. Even though the shell cracked and the column lost part of its full capacity, the specimen still showed sufficient strength and behaved like a conventional reinforced concrete column with the steel cage located in the normal strength concrete core completely intact.

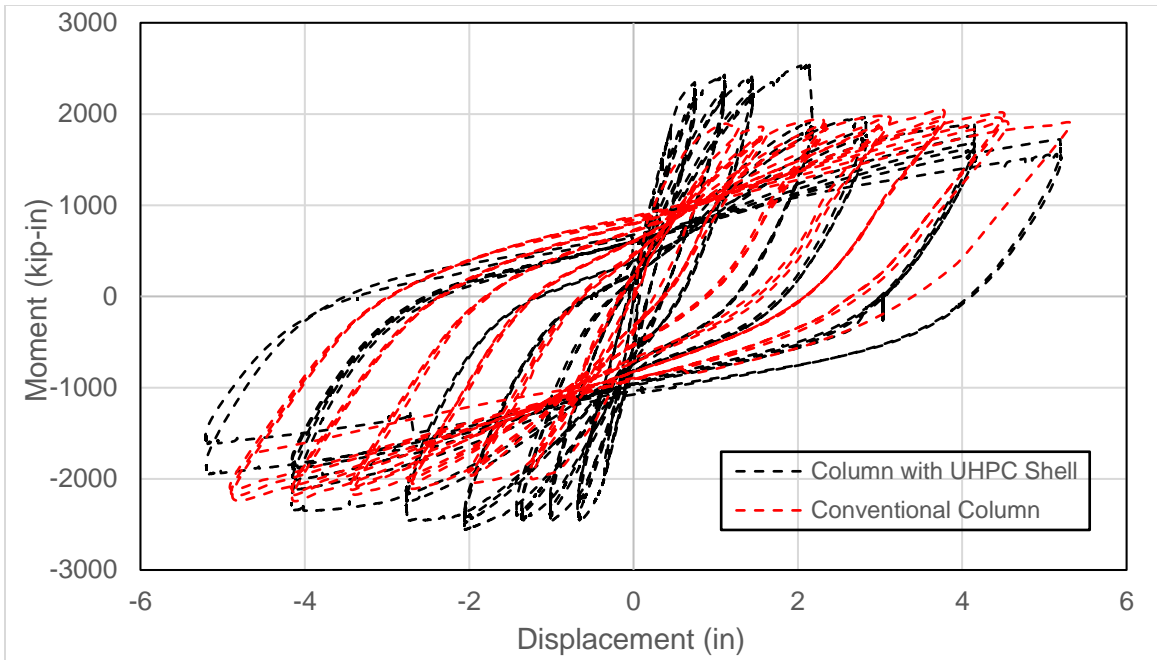


Figure 5-2 Moment-displacement response of the first specimen and the conventional column specimen.

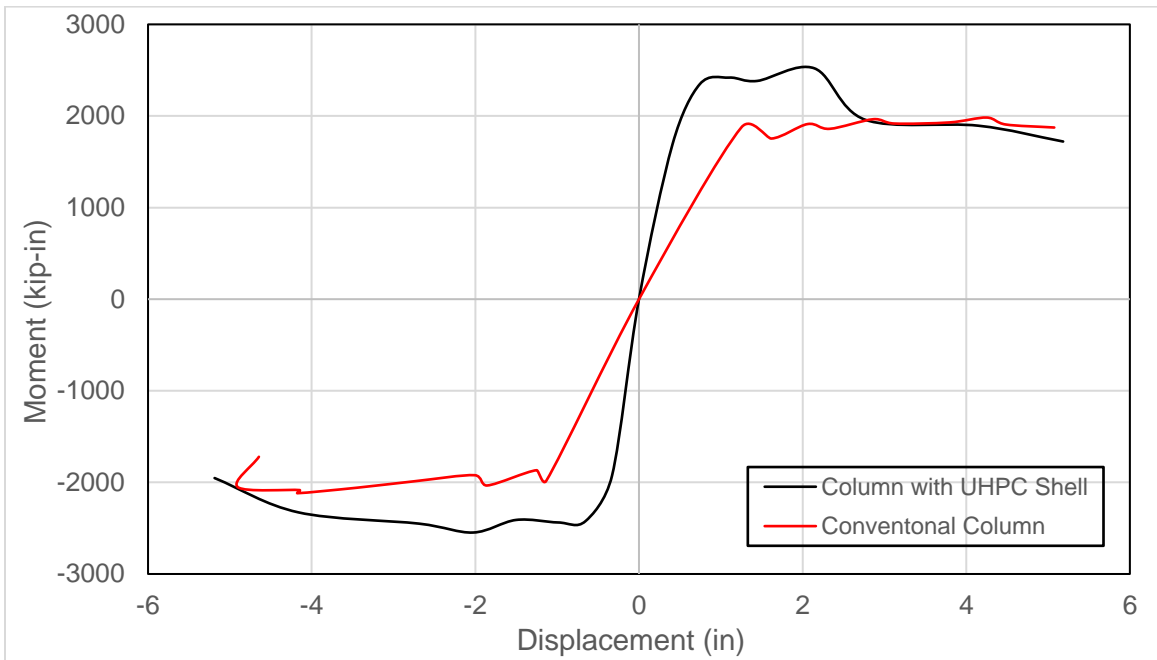


Figure 5-3 Comparison of response envelopes of the first specimen and the conventional column specimen.

5.1.3 Drift-Rotation Response of the First Specimen

As mentioned in Chapter 4, the UHPC step was instrumented with four displacement transducers at all four directions in order to collect the rotation data between the UHPC step and the footing. Based on rotation results, the rotation between the UHPC step and the footing was negligible and can be considered zero which means that the UHPC step never rotated and the splice length of the longitudinal bars with the dowel bars was sufficient to prevent cracking of the footing. Based on the damage observations, large crack that occurred between the column and the UHPC step indicated that the rotation was concentrated at the interface between the UHPC step and the column. In order to confirm this observation, the rotation at the interface between the column and UHPC step was calculated by subtracting the measured displacement in the two opposite displacement transducers then dividing the result by the direct horizontal distance of 21 in. The drift-rotation response is shown in Figure 5-4. By comparing the rotation at the interface between the column with UHPC shell and the UHPC step to rigid body rotation, it can be concluded that the rotations were mostly concentrated at the interface between the UHPC step and the column. Figure 5-4 only depicts the results up to 2-3% drift ratio due to the damage of the shell at higher drift ratios which affected the functionality of the displacement transducers and made them erroneous.

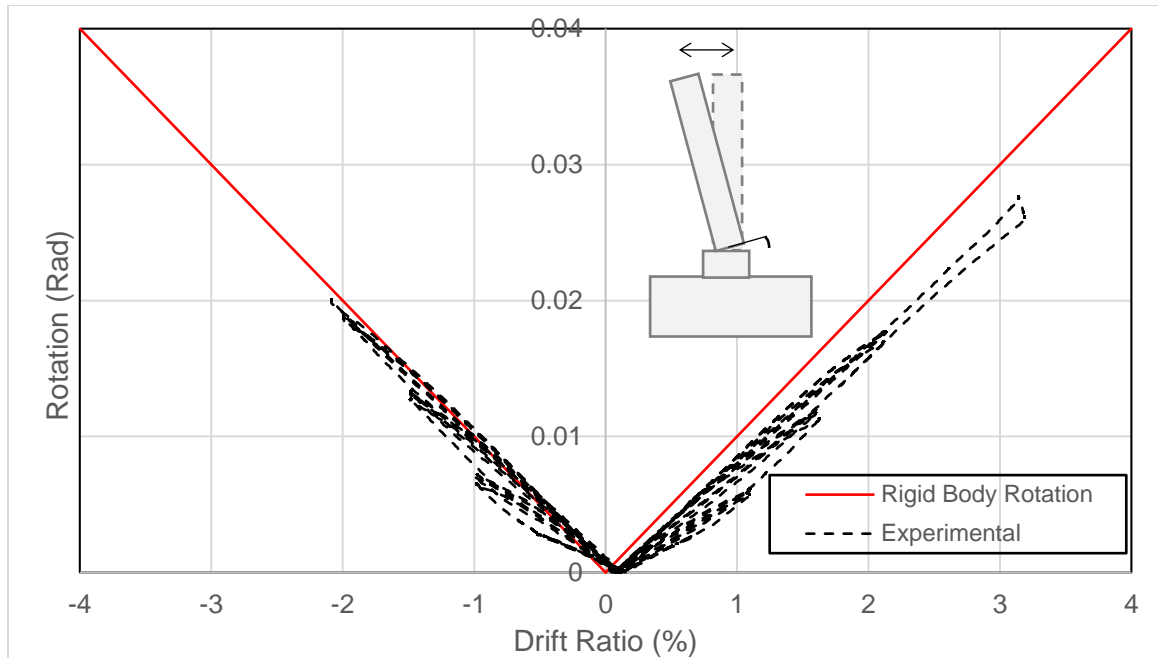


Figure 5-4 Drift-rotation response of the first specimen.

5.1.4 Energy Dissipation

The energy dissipation graph was developed by calculating the area of each hysteresis loop in force-displacement curve for each cycle at each drift ratio. Since each drift ratio had three cycles, except the 6% drift ratio, the values of all three values were averaged and used to plot the graph which is shown in Figure 5-5. It can be observed that the first specimen had a linear energy dissipation trend until the 2-3% drift ratio when the UHPC shell has cracked. After the cracking of the UHPC shell, the conventional reinforced concrete member dissipated energy due to the inelastic behavior at higher drift ratios. At higher drift ratio, the first specimen acted as conventional column with energy dissipation due to the inelastic deformation of the reinforcing bars. Higher energy dissipation is always desirable during earthquakes events.

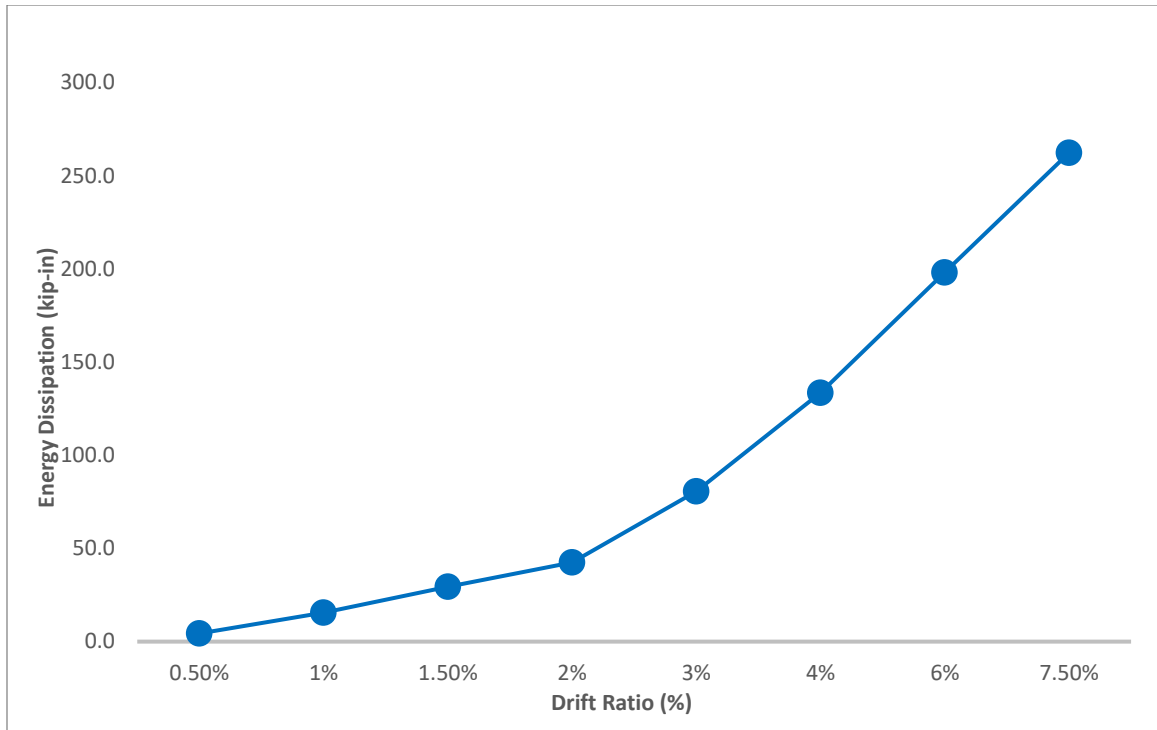


Figure 5-5 Energy dissipation at each drift level of the first specimen.

5.1.5 Residual Drift

In order to fully understand the performance of a structural system and the sustained damage after the application of cyclic loading, residual drifts need to be calculated. Residual drift represents the damage degree of the structure while also reflecting the post-earthquake reparability of the structure. Using the data gathered from the testing of the first specimen, a tradeline was plotted that shows the residual drift after each drift ratio. Since three cycles were applied for each drift ratio, the average value was calculated and used in Figure 5-6. From Figure 5-6, residual drifts were small values up to 1.5% drift ratio and increased at higher drift ration due to the specimen damage. The residual drift increased to 6% at the 7.5% drift ratio after which the testing was completed due to the rebar rupture. Higher residual drifts reflect the damage progression. This first specimen experienced

higher drift ratio due to the mode of failure by cracking the UHPC shell at the interface between the column and the UHPC step.

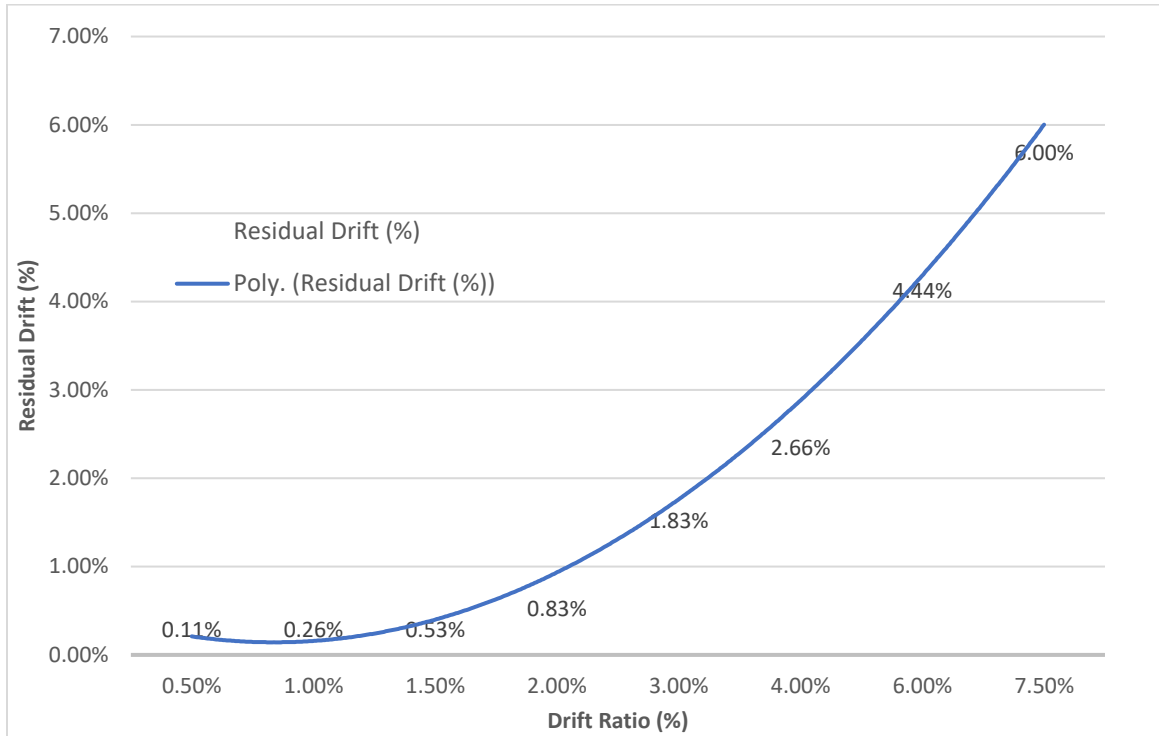


Figure 5-6 Residual drift after each drift ratio application for the first specimen.

5.1.6 Strain Response

For the first specimen, 24 strain gauges were used to measure strains in both longitudinal reinforcement and dowel bars. In order to display the strain progression, a strain distribution plot was developed for the North bar of the first specimen at 1% and 2% drift ratios at different column heights, as shown in Figure 5-7. Two strain gauges, instrumented on the dowel bars at 2 in. and 4 in. below the footing interface, show similar strain values less than yield strain for both drift ratios. These values show that the dowel bars located inside the footing confirm that the footing never cracked which was a requirement for capacity protected elements. Furthermore, another three strain gauges were

located on the longitudinal reinforcement of the steel cage, on the same side, 7 in, 11.5 in. and 16. above the footing interface in order to compare the strain values at 1% and 2% drift ratios. Based on Figure 5-7, the strain gauges located at the height of 7 in. above the footing showed the most visible change of the strain values which proves that the plastic hinge was shifted to be above the UHPC step away from the critical section at the footing-to-column interface. The strain gauge located at 11.5 in. above the footing interface was lost before applying 2% drift ratio, so the results are not applicable.

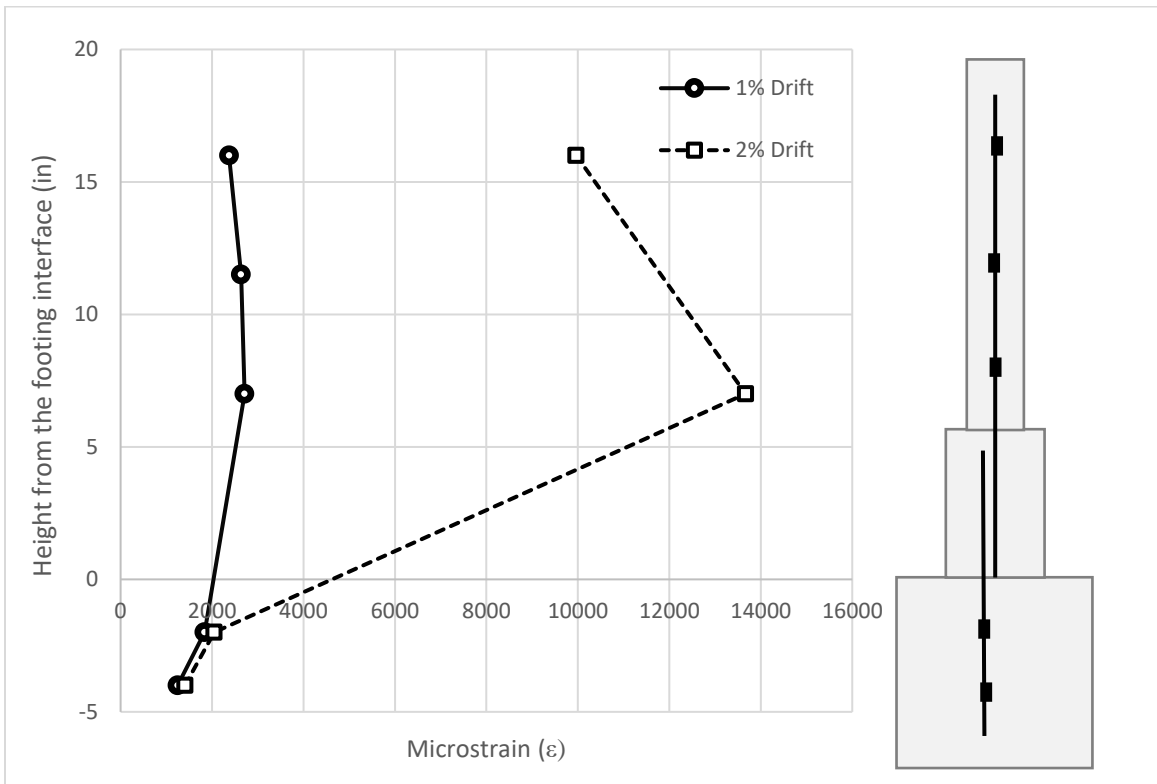


Figure 5-7 Strain distribution on the north longitudinal and dowel bars for first specimen.

5.2 Results for the Second Specimen

5.2.1 Damage Progression

The testing of the second specimen started by applying many cycles of lateral load equals 10 kips at both loading directions (pushing from North to South, pulling from South to North) to determine the initial stiffness of the system. After the trial run, the actual testing started by applying a drift ratio of 0.5% which corresponds to a lateral displacement of 0.34 in. When pushing the column from North to South, a lateral load of 29.5 kips was recorded that caused the targeted displacement of 0.34 in. By pulling the column on the opposite side, the lateral load slightly increased to 33 kips. For the second and third cycles, loads of 28 kips and 32 kips were recorded when pushing and pulling the specimen, respectively. Only minor cracks were noticed and were located around the UHPC shell at the interface between the UHPC shell and the UHPC step, as shown in Figure 5-8a.

The next drift ratio corresponding to 1% (displacement of 0.68 in.) was applied in both loading directions where a lateral load of 35.5 kips was recorded on the positive side (pushing from North to South). However, on the negative side (pulling from South to North), the lateral load was slightly higher by 4.5 kips (40 kips). For the second and third cycles corresponding to the same drift ratio, lateral loads of 33 kips and 38.5 kips were recorded on the positive and negative sides, respectively. The progression of the existing cracks and formation of new ones were observed while a major horizontal crack was noticed 1 in. above the interface between the UHPC step and the column, on the north side of the specimen, as shown in Figure 5-8b. This crack was a structural crack due to the

cyclic loading, however, a minor crack was observed on the South side for the same drift ratio.

A drift ratio of 1.5% (displacement of 1.02 in.) was applied. On the positive side (pushing from North to South), the recorded lateral load was approximately 35 kips for all three cycles, however, for the negative side (pulling from South to North), the recorded lateral load was significantly higher with a recorded value of 42.5 kips for the first cycle, and 41 kips for the second and third cycles. The major crack on the North side continued to extend and widen, as shown in Figure 5-8c with the steel fiber exposure, however, a slight progression of cracks was noticed on the South side located at the interface between the UHPC shell and UHPC step. Furthermore, new vertical cracks were observed on the UHPC step starting from the top. These cracks seemed to be symmetrically distributed around this section between the dowel bars (second set of dowel bars).

A drift ratio of 2% (displacement of 1.37 in.) was applied. During the first cycle, a lateral load of 37 kips was recorded on the positive side (pushing from North to South) and 41.5 kips was recorded on the negative side (pulling from North to South). In the second cycle, loads of 35 and 37 kips were applied at the positive and negative side, respectively. In the third cycle, a lateral load of 33 kips was recorded at both sides. Further progression of the major crack on the North side was observed causing the exposure column spiral located in the UHPC shell and causing minor UHPC spalling on both sides of the specimen. The cracks on the UHPC step continued to grow especially when the cracks experienced tension forces which are visible on the video records, as shown in Figure 5-8d. It should be mentioned that the major crack that started on the North side, just below the bottom

potentiometer, continued to grow around the perimeter of the shell in a downward direction.

A drift ratio of 3% (displacement of 2.1 in.) was applied. For the first cycle, lateral loads of 34 kips on the positive side (pushing from North to South) and 31 kips on the negative side (pulling from South to North) were recorded. During the second and third cycles, lateral loads dropped to 27 kips and 25 kips for the positive and negative sides respectively. Therefore, lateral capacity dropped by 27% and 40% for the positive and negative sides, respectively. During this drift ratio, once the specimen was pulled from South to North, sliding of the cracked pieces of UHPC shell was observed causing further spalling and degradation of the UHPC shell. Due to the premature shell failure, and probable detachment between the longitudinal reinforcement, normal strength concrete and UHPC in the column, the shear capacity of column section dropped significantly causing the transfer of shear forces to the UHPC step with progression in cracks in the UHPC step, as shown in Figure 5-8e.

Even though the lateral load capacity continued to drop, the test was resumed on by applying a drift ratio of 4% (displacement of 2.73 in.). Lateral loads of 22 kips and 25 kips were recorded for the first cycle on the positive and negative sides, respectively. The load started to drop even more for the second and third cycles, reaching the values of 19 kips and 23 kips for the second cycle, and 17.5 kips and 22.5 kips for the third cycle on the positive and negative sides, respectively. During these cycles, further spalling of the UHPC shell, as shown in Figure 5-8f was observed causing reduction in the area of the column section leading to lower lateral load capacity.

A drift ratio of 5% (displacement of 3.41 in.) was applied. In the first cycle, lateral loads of 18 kips for the positive side (pushing from North to South) and 23 kips for the negative side (pulling from South to North) were recorded. During the second and third cycles, the lateral load dropped to 16 kips and 21 kips for the positive and negative sides, respectively. The lateral load capacity of this specimen dropped by almost 50% at this drift ratio. The large horizontal crack progressed diagonally, as shown in Figure 5-8g. It was observed that the longitudinal reinforcement inside the specimen was exposed, however, no bar rupture was noticed.

Even though the specimen was considered failed due to the significant loss in lateral load capacity during the application of 5% drift ratio, one last loading was conducted with a drift ratio of 6% (displacement of 4.1 in.). Lateral loads of 17 kips were recorded on the positive side and 21 kips on the negative side. The larger crack on the north side opened slightly more, as shown in Figure 5-8h, while the vertical cracks on the UHPC step became even more visible. At this stage, it was decided that the test should be ended due to the significant loss in lateral load capacity. The summary of damages and corresponding maximum lateral loads are listed in Table 5-2.

Table 5-2 Summary of applied loads and corresponding key damage states for second specimen.

Displacement Ductility	Number of Cycles	Drift Ratio	Maximum Lateral Load	Key Damage Stage
Δ_y	3	0.5%	29.5 kips (N to S) 33 kips (S to N)	Minor cracks around the UHPC shell
$2\Delta_y$	3	1%	35.5 kips (N to S) 40 kips (S to N)	Progression of minor cracks around the UHPC Shell (mostly on north side)
$3\Delta_y$	3	1.5%	35 kips (N to S) 42.5 kips (S to N)	Further opening of exiting cracks Steel fibers were noticed
$4\Delta_y$	3	2%	37 kips (N to S) 41.5 kips (S to N)	Large cracks and spalling, extensive damage on the north side and minor cracks on the UHPC step
$6\Delta_y$	3	3%	34 kips (N to S) 31 kips (S to N)	Shell cracked at north side Damage concentrated 2in. above the UHPC Shell and Step interface on the north side
$8\Delta_y$	3	4%	22 kips (N to S) 25 kips (S to N)	Large, symmetrical cracks on the UHPC step. Extensive damage on the Interface between the Column and UHPC step
$10\Delta_y$	3	5%	18 kips (N to S) 23 kips (S to N)	Large opening between column and UHPC shell, and even larger openings of the cracks on UHPC step
$12\Delta_y$	1	6%	17 kips (N to S) 21 kips (S to N)	Sliding of the cracks on the UHPC shell, extensive damage of the UHPC step, no rebar rupture

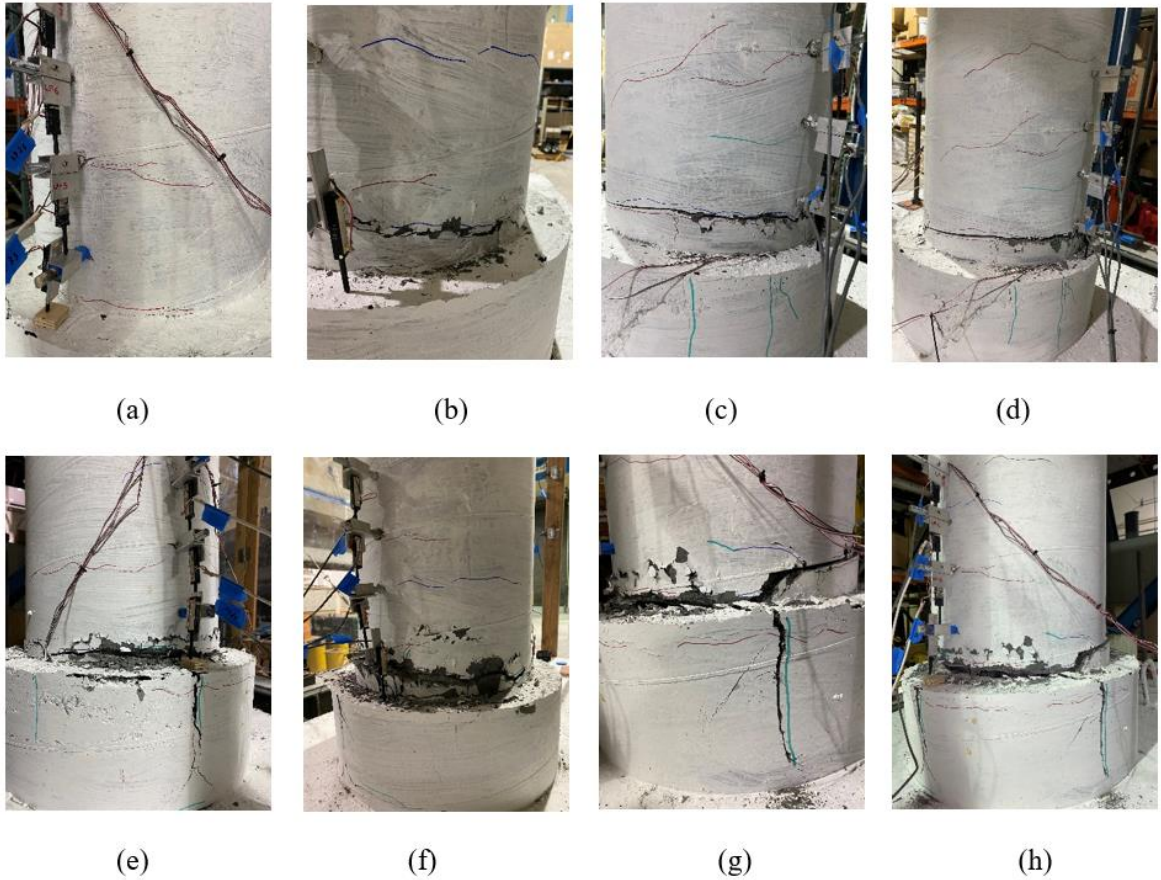


Figure 5-8 Damage progression of the second specimen: a) 0.5% drift ratio; b) 1% drift ratio; c) 1.5% drift ratio; d) 2% drift ratio; e) 3% drift ratio; f) 4% drift ratio; g) 5% drift ratio; h) 6% drift ratio.

5.2.2 Moment-Displacement Response

Using the collected data from the instruments for the second specimen test, moment-displacement hysteresis loops for the cyclic response was developed, as shown in Figure 5-9. For comparison purposes, Figure 5-9 also shows the same results for the first specimen where no longitudinal reinforcing bars were shared between UHPC shell and normal strength concrete core. Based on the figure, it can be observed that the second specimen acted poorly if compared to the first specimen due to the significant loss in lateral load capacity. The behavior of both columns was similar, with the almost matching moment

capacity up to a displacement of 1.4 in. (2% drift ratio). After 2% drift ratio, the moment capacity (lateral load capacity) of the second specimen started to drop, leading to the conclusion that the UHPC shell failed around this drift ratio. Further testing showed that the stiffness of the second specimen significantly dropped leading to the conclusion that the specimen has failed. The same behavior was presented in Figure 5-10, which shows the response envelopes of the first and second specimen. At the last cycle of 6% drift ratio, the moment capacity was half of its full capacity that was reached at the drift ratio at 2%. It can be noticed that the second specimen experienced lower residual drift due to the loss in lateral load capacity. Lower residual drifts are desirable except when restoring forces (re-centering forces, for example) are not presented in the system. In this case, the lower residual drifts reflect the significant loss in lateral load capacity.

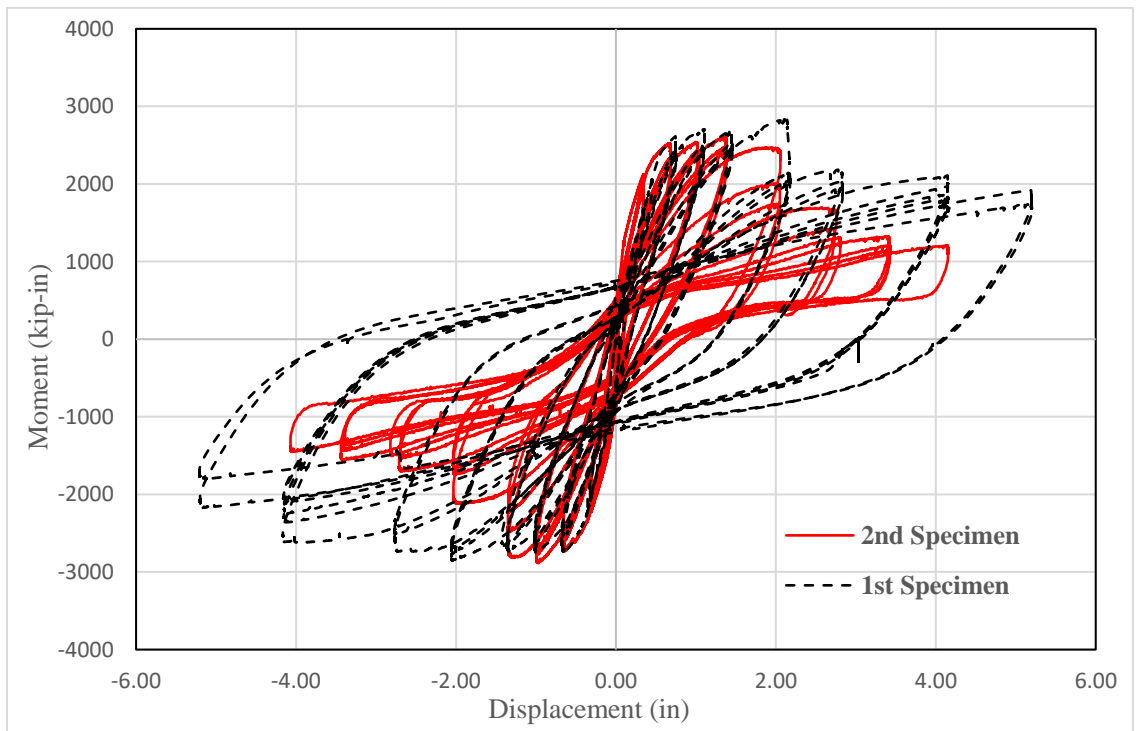


Figure 5-9 Moment-displacement response of the second specimen and the first specimen for comparison.

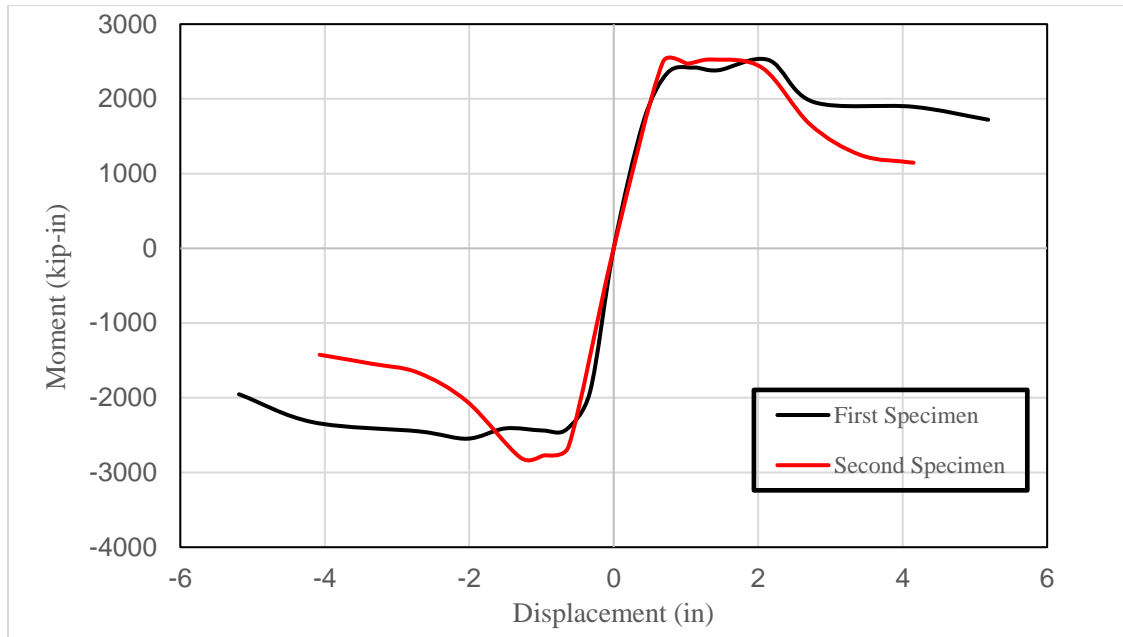


Figure 5-10 Comparison of response envelopes for both specimens.

5.2.3 Drift-Rotation Response

For the second specimen, no rotation was noticed between the UHPC step and the footing and has been taken as zero, same as the first specimen. Eight displacement transducers, four on the North and four on the South side, were placed to record the rotation of the column section since the major crack was expected to occur around the interface between the UHPC step and the column similar to the first specimen. Figure 5-11 shows the drift vs. rotation response of the second specimen. The drift-rotation response was plotted in a similar manner as Figure 5-4. It can be noticed that the positive side (pushing from North to South) has a higher slope which can be explained by the appearance of the major crack 1 in. above the UHPC step on the north side. This indicates that the larger rotations were recorded on the north side. Since the tipping point on the North side is 1 inch higher than the tipping point on the south side, the peak of the plot shown in Figure

5-11 on both North and South sides becomes significantly less steep between the 5% and 6% drift ratio. This behavior means that the damaged part has slid once the lateral load was applied causing higher drift ratio but no additional rotation. This sliding also can explain why the drift-rotation slopes exceeded the theoretical rigid body rotation in this plot.

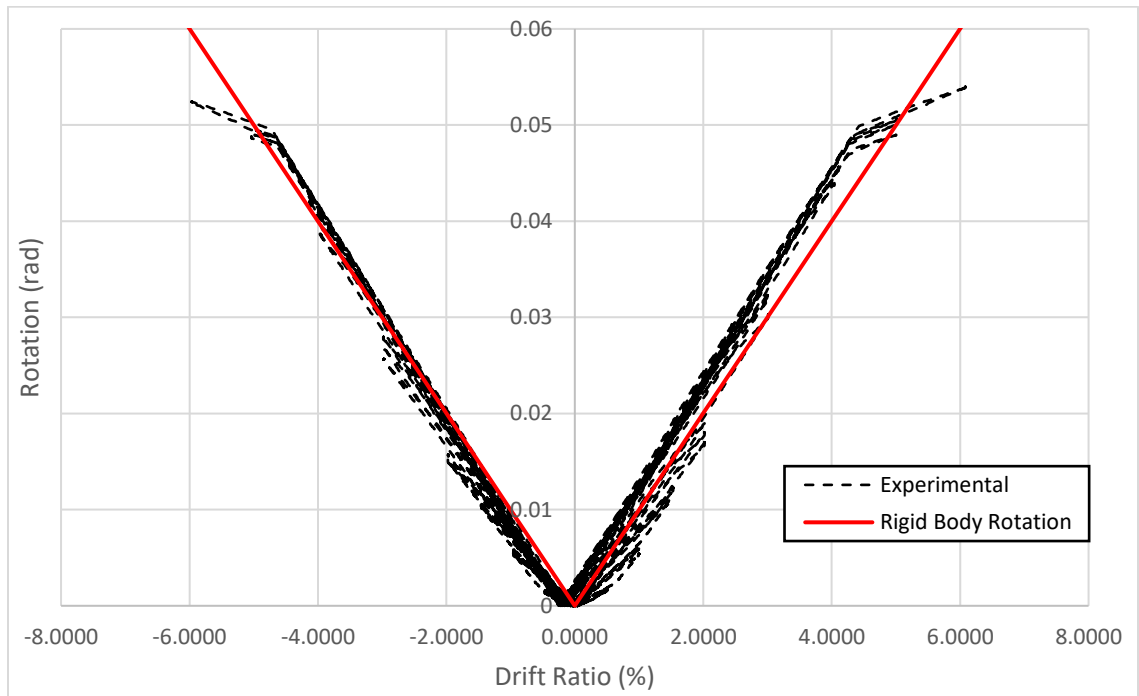


Figure 5-11 Drift-rotation response for the second specimen.

5.2.4 Energy Dissipation

After the testing of the second specimen, Figure 5-12 was developed to show energy dissipation trends for both the first and second specimens for comparison purposes. Up to 2% drift ratio, the second specimen behaved identically to the first specimen. However, after the UHPC shell cracked and spalled, the energy dissipation does not follow the trend path as the first specimen due to the difference in premature failure. The energy dissipation values remained almost constant up to 6% drift ratio when the testing was terminated due

to significant loss in lateral load capacity. Bridge columns in seismic regions are designed to absorb energy and to dissipate it in forms of plastic deformation such as concrete cracking and spalling and reinforcing bar deformations such as plastic strains and buckling. The second specimen was not able to dissipate energy as shown in Figure 5-12 and slim area of hysteresis loops in Figure 5-9. Since the lateral load capacity dropped significantly due to section losses, longitudinal reinforcing bars did not experience large deformation to assist in dissipating more energy.

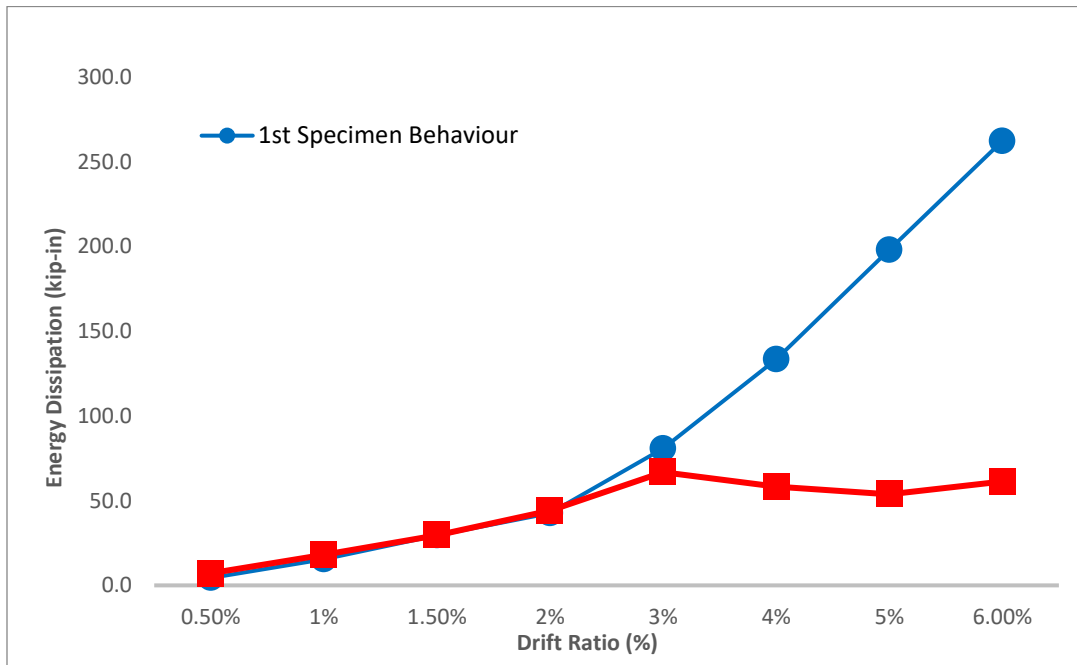


Figure 5-12 Energy dissipation comparison of both specimens.

5.2.5 Residual Drift

Figure 5-13 shows the residual drift ratio corresponding to each drift level in the same manner for the first specimen. However, the results were different due to the different design and reinforcement placement in the UHPC shell column, showing lower lateral load

capacity right after the UHPC shell has cracked and spalled. As it can be noticed from Figure 5-13, the trend is significantly different from the first specimen. The residual drift values are similar to the first specimen up to 2%, when the UHPC shell of the second specimen has cracked and started to spall. Lower residual drifts are desirable except when restoring forces (re-centering forces, for example) are not presented in the system. In this case, the lower residual drifts reflect the significant loss in lateral load capacity.

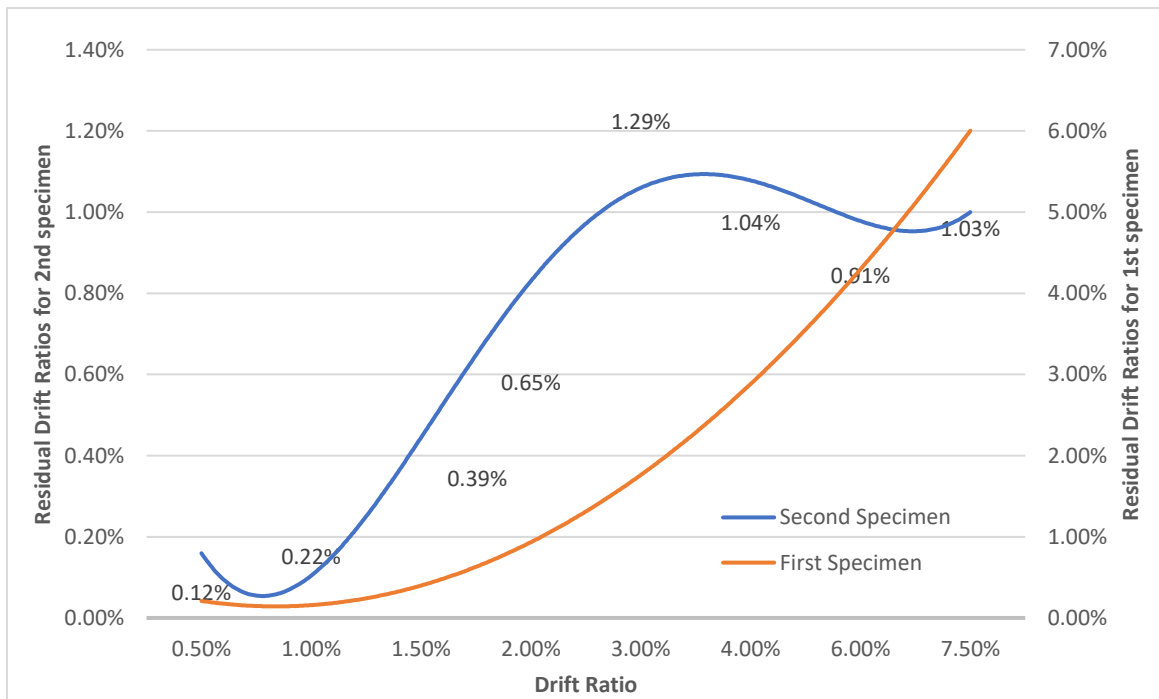


Figure 5-13 Residual drift ratio for the second specimen and the comparison to the first specimen.

5.2.6 Strain Response

For the second specimen, 16 strain gauges were attached to both the dowel bars and longitudinal reinforcement to measure reinforcement strains. A strain distribution plot was developed for the South bar of the second specimen for drift ratios of 1% and 1.5% at

different column heights, as shown in Figure 5-14. The three strain gauges located on the South dowel bar at 1 in., 4 in. and 6 in. below the footing interface recorded similar strains below the yield strain. The strains in the South dowel bar increased slightly from 1% to 2% drift ratio indicating that the design was appropriate in preventing the cracking of the footing which is a capacity protected element. Furthermore, another three strain gauges were attached to the South longitudinal reinforcing bar at 8 in., 13 in., and 18 in. above the footing interface. Based on the plot shown in Figure 5-14, the strain gauges located at the height of 8 in. showed the most noticeable change in their strain values. However, it is typically very tough to monitor and receive correct strain gauge values at higher displacement due to their damage or wire damages which can be observed for the strain gauge located at 18 in. above the interface.

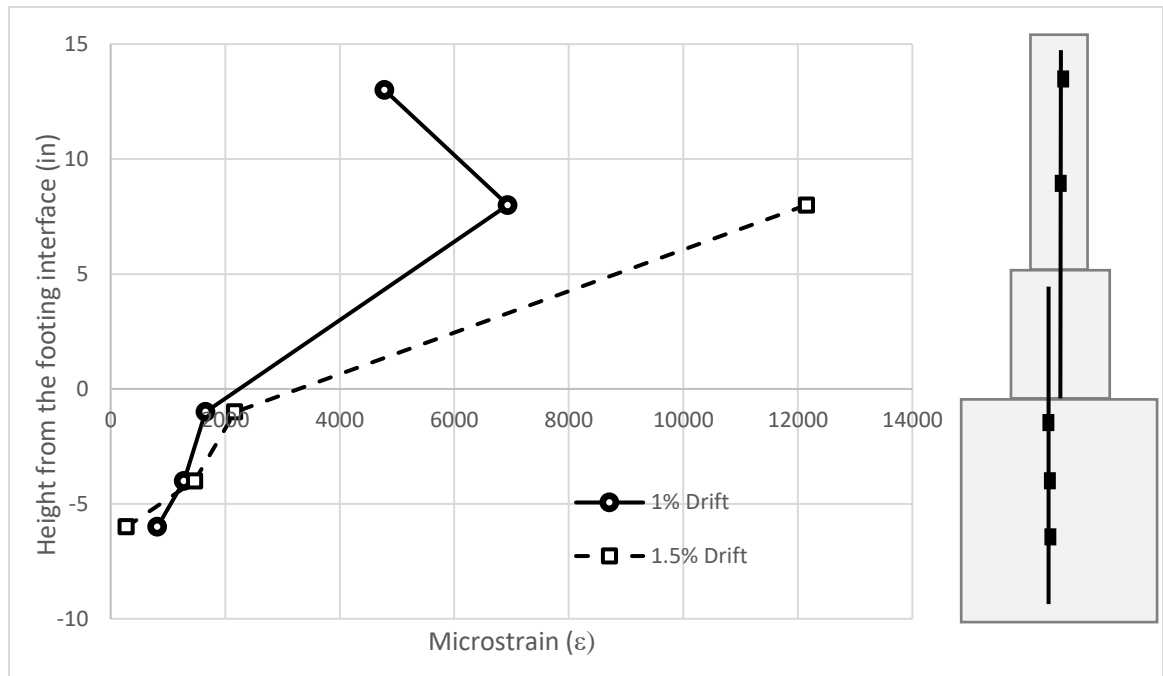


Figure 5-14 Strain distribution on the south longitudinal and dowel bar for the second specimen.

6 SUMMARY AND CONCLUSIONS

In this research, two specimens were tested to establish the effectiveness of the prefabricated UHPC shell concept for circular bridge columns. This concept was suggested in order to eliminate conventional formwork and reduce scaffolding that is typically used during construction to decrease traffic congestion and on-site construction time. In addition, the UHPC shell acts as a protective layer for the normal strength concrete inside.

The first specimen was designed and constructed so the UHPC shell is not reinforced with any longitudinal or transverse reinforcement and column reinforcement were placed inside the shell cavity prior to casting the normal strength concrete. The second specimen was designed and constructed so that the transverse reinforcement (spiral) is totally embedded in the UHPC shell and the longitudinal reinforcing bars are equally shared between the UHPC and normal strength concrete aiming to increase the bond between the shell and normal strength concrete inside it. Both shells were connected to their footing using a step made of UHPC to shorten the length of the extended dowel bars from the footings.

Both specimens were tested by applying a constant axial load of 120 kips and incremental cyclic loads until failure. Seven different drift ratios were applied on the first specimen when the first reinforcing bar fractured at 7.5% whereas eight different drift ratios were applied on the second specimen when the test stopped completed at a drift ratio of 6% due to the significant drop of lateral load capacity of more than 50% even without any reinforcing bar ruptures.

The designed UHPC step element helped to successfully shift the plastic hinge away from the column-to-footing interface. The first specimen showed no damage in the UHPC step element, while the second specimen developed vertical cracks caused by the lack of transverse reinforcement in the UHPC step. The damage in the UHPC step of the second specimen can be mitigated using transverse reinforcement in the step.

For the first specimen, the main cracks started to appear in the south and north sides of the column, at the connection between the column and the top of the UHPC step, where the bar rupture happened. In this case, even when the UHPC shell had cracked at the north side at the 3% drift ratio, the column still had a significant capacity to resist the displacement 15 times the yield displacement, which corresponds to 7.5% drift ratio.

The second specimen showed similar behavior as the first specimen up to a drift ratio of 2% after which its stiffness and lateral load capacity dropped drastically ending up with the half of its maximum lateral load capacity at the drift ratio of 6%.

From the conducted tests, the following conclusions can be drawn:

- For the first specimen, the design of the UHPC step was successful in shifting the plastic hinge away from the column-to-footing interface by increasing the flexural strength of this area. For the second specimen, before achieving 2% drift ratio, the UHPC step was successful in shifting the plastic hinge away from the critical column-to-footing interface. However, vertical cracks at the UHPC step were observed indicating the need for transverse reinforcement around the dowel bars in the UHPC step.

- Even though the UHPC shell has cracked at 3% drift ratio for the first specimen, the column specimen still showed a significant lateral load capacity, continuing to behave like a conventional reinforced concrete column. Once the second specimen reached 2% drift ratio, the lateral load capacity has significantly dropped in comparison to the first specimen.
- Up to 2% drift ratio, energy dissipation values of the second specimen matched those calculated from the first column; however, energy dissipation values were much lower for higher drift ratio.
- Residual drift values were lower for the second column than those calculated from the first column. Even though lower residual drift ratios are preferable, in this case, they indicate that the second specimen lost significant lateral load capacity, became “loose”.
- No slippage was noticed between the UHPC shell and the normal concrete core, while also no rotation or damage in UHPC step element was noticed for the first specimen.

In order to better understand the behavior between the UHPC shell and normal strength concrete core with or without embedded longitudinal reinforcement, further testing is needed. For future testing, additional transverse reinforcement needs to be considered for the UHPC step element, together with the behavior of the embedded longitudinal bars between the normal strength concrete and UHPC since their bonds are acting differently when the same loading is applied.

REFERENCES

- [1] Infrastructure Health & Safety Association (IHSA), The Construction Health and Safety Manual, Chapter 42. Ontario, Canada, 2017.
- [2] Barbosa, A.; Gambatese, J.; Das, A; Pestana, A.C. Mapped Workflow for Safety and Reliability and Reliability Assessments of Use and Reuse Formwork. *Construction Research Congress 2014*, 2014.
- [3] Mothokho, L.; Emuze, F.; Aka A. Formwork and Falsework Hazards in Construction: Status and Effects in Bloemfontein, South Africa. *Proceedings of the 2015 (6th) International Conference of Engineering, Project, and Production Management*.
- [4] Vibin, R.; Ilango, S.P. Risk Assessment and Safety in Formwork. *Two Day National Conference on Civil Structure and Environmental Engineering*. 2015.
- [5] Caluk, N., Mantawy, I., & Azizinamini, A. (2019). Durable Bridge Columns using Stay-In-Place UHPC Shells for Accelerated Bridge Construction. *Infrastructures*, 4(2), 25.
- [6] Caluk, Nerma, et al. "Cyclic Test of Concrete Bridge Column Utilizing Ultra-High Performance Concrete Shell." *Transportation Research Record*, Feb. 2020, doi:10.1177/0361198120906088.
- [7] Azizinamini, A., Rehmat, S., & Sadeghnejad, A. (2019). Enhancing Resiliency and Delivery of Bridge Elements using Ultra-High Performance Concrete as Formwork. *Transportation Research Record*, 0361198119834907.
- [8] Haber, B.; De la Varga, I. ; Graybeal, B.; Nakashoji, B.; El-Helou, F. Properties and Behavior of UHPC-Class Materials. No. FHWA-HRT-18-036. United States. *Federal Highway Administration. Office of Infrastructure Research and Development*, 2018.
- [9] Valikhani, A., Jahromi, A. J., Mantawy, I. M., & Azizinamini, A. (2020). Experimental evaluation of concrete-to-UHPC bond strength with correlation to surface roughness for repair application. *Construction and Building Materials*, 238, 117753.
- [10] ASTM C1856 / C1856M-17, Standard Practice for Fabricating and Testing Specimens of Ultra-High Performance Concrete, ASTM International, West Conshohocken, PA, 2017

- [11] Valikhani, A., Jaberi, A. J., & Atorod, A. (2018). Experimental Investigation of High-Performance Protective Shell Used for Retrofitting Bridge Elements. *Transportation Research Board*, 01658080.
- [12] Valikhani, A., Jaberi, A. J., & Atorod, A. (2016). Retrofitting Damaged Bridge Elements Using Thin Ultra High Performance Shell Elements. *Transportation Research Board*, 01626600.
- [13] Stephens M.T., Berg L., Lehman D.E., Roeder C.W. (2014). Concrete-Filled Tubes for Accelerated Bridge Construction. *Transportation Research Board, Vol 2406, Issue 1*.
- [14] Stephens M.T., Berg L., Lehman D.E., Roeder C.W. (2015). Concrete-Filled Bridge Pier Connections for Accelerated Bridge Construction. *California Department of Transportation*, No. 65A0446.
- [15] Mingzhang L., Weijie L., Chuang H., Gangbing S. (2016). Concrete Infill Monitoring in Concrete-Filled FRP Tubes Using a PZT-Based Ultrasonic Time-of-Flight Method. *Sensors* 2016.
- [16] Asmaa A. A., Masmoudi R. (2018). Axial Response of Concrete-Filled FRP Tube (CFFT) Columns with Internal Bars. *Journal of Composite Science*, 2018.
- [17] The Architects Newspaper, URL: <https://archpaper.com/2018/08/bridge-maintenance-us/>, 2018.
- [18] Russell, H.; Graybeal, B. Ultra-High Performance Concrete: A State-of-the-Art Report for the Bridge Community. No. FHWA-HRT-13-060. United States. *Federal Highway Administration. Office of Infrastructure Research and Development*, 2013.
- [19] Farzad, M., Fancy, Saiada F., Lau, K., Azizinamini, A. Chloride Penetration at Cold Joints of Structural Members with Dissimilar Concrete Incorporating UHPC.
- [20] Shafieifar, M. Alternative ABC Connecting Precast Column to Cap Beam Using UHPC. *Accelerated Bridge Construction University Transportation Center ABC-UTC*. 2018.
- [21] Graybeal B. Bond Behavior of Reinforcing Steel in Ultra-High Performance Concrete. No. FHWA-HRT-14-089. United States. *Federal Highway Administration. Office of Infrastructure Research and Development*, 2014

- [22] A. Sadeghnejad, R. Taghinezhadbilondy, and A. Azizinamini. "Seismic Performance of a New Connection Detail in an SDCL Steel Bridge System." *Journal of Bridge Engineering* 24.10 (2019): 04019094.